AD-A131 032 JOURNAL OF THE CHINESE SOCIETY OF ASTRONAUTICS (SELECTED ARTICLES)(U) FOREIGN TECHNOLOGY DIV WRIGHT-PATTERSON AFB OH Y JIACHI ET AL. 01 JUL 83 1/1

UNCLASSIFIED FTD-ID(RS)T-0373-83 F/G 22/2 NL

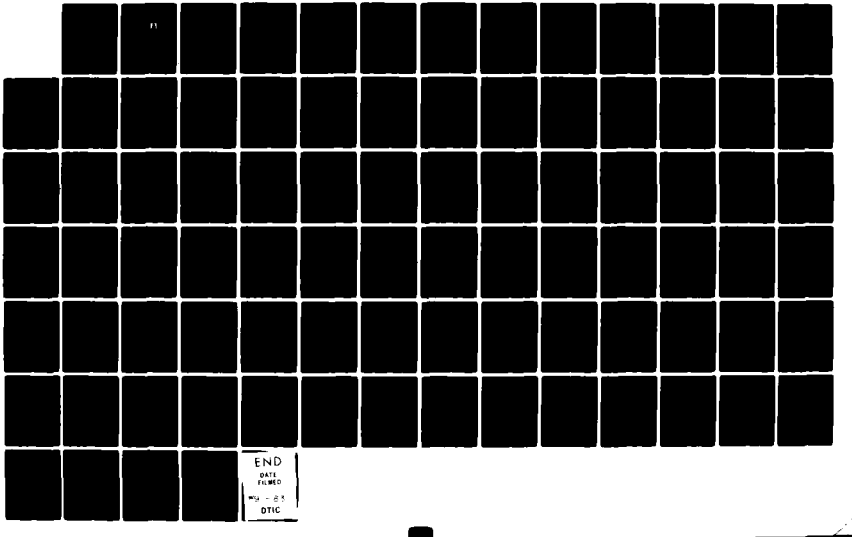

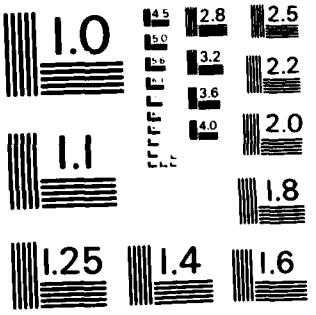

FTD-ID(RS)T-0373-83

AD A131032

FOREIGN TECHNOLOGY DIVISION

JOURNAL OF THE CHINESE SOCIETY OF ASTRONAUTICS

(Selected Articles)

Approved for public release;
distribution unlimited.

83 08 3 .213

EDITED TRANSLATION

FTD-ID(RS)T-0373-83 1 July 1983

MICROFICHE NR: FTD-83-C-000800

JOURNAL OF THE CHINESE SOCIETY OF ASTRONAUTICS
(Selected Articles)

English pages: 81
Source: Yuhang Xuebao, Nr. 1, Beijing, 1981,
pp. 1-13; 23-30; 31-41; 66-75; 84-91

Country of origin: China
Translated by: SCITRAN
F33657-81-D-0263
Requester: FTD/SDSY

PREPARED BY:

TRANSLATION DIVISION
FOREIGN TECHNOLOGY DIVISION
WP-AFB, OHIO.

A

Table of Contents

GRAPHICS DISCLAIMER

All figures, graphics, tables, equations, etc. merged into this translation were extracted from the best quality copy available.

ATTITUDE CONTROL SYSTEM OF RECOVERABLE EARTH-ORIENTING TECHNOLOGY TESTING SATELLITES AND SOME FLIGHT TESTING RESULTS

Yang Jiachi, Zhang Guofu, Sun Chengqi, Feng Xueyi and Niu Yinsheng*

(Beijing Institute of Control Engineering)

ABSTRACT

In 1970, three recoverable technology testing satellites, permitting orientation of observatory with respect to the earth, were successfully launched, operated in orbit and recovered. This paper reviews the three-axis stabilized attitude control system used in these satellites, including its composition, function and considerations of selecting main parameters in the system, etc. Finally the opening performances of the flight testing results are briefly described.

I. INTRODUCTION

A first generation three-axis stabilized attitude control system was first used on recoverable technology testing satellites permitting orientation of observation with respect to the Earth and successfully accomplished the following tasks:

Eliminating the initial satellite attitude aberration caused by the separation of the launch vehicle from the satellite:

assuring the attitude precision and the attitude angular velocity requirement needed for satellite observation of the Earth during the orbitting period;

enabling the satellite to achieve the attitude required for recovery by rapidly rotating about the yaw axis before returning to Earth.

In this paper, we emphasize the introduction of the structure, the mechanism and the design for the principal parameters of the attitude control system. Finally, the analysis of the result of the flight tests is briefly described.

---

*Received March 26, 1980

II. DESCRIPTION OF THE ATTITUDE CONTROL SYSTEM AND THE CONSIDERATION FOR THE CHOICE OF THE PRINCIPAL PARAMETERS

The attitude control system is formed of the attitude measurement system, the central control circuits and the propulsion execution mechanism through the satellite closed circuit. The description of the attitude movement is based upon the Earth-centered orbital coordinate system and the satellite coordinate system as shown in Figure 1. The angles between the two systems are denoted as ϕ, θ and ψ, respectively called the roll attitude angle, the pitch attitude angle and the yaw attitude angle.

1. The attitude measurement system

In order to establish the Earth-centered orbital coordinate system in the orbit as a standard for measuring the satellite attitude and to give the signal for attitude deviation while being able to satisfy the requirement of eliminating the initial attitude deviation and establishing the return attitude, we have selected an attitude measurement system composed of two conical scanning infrared level meters and two gyros with two-three degrees of freedom. As shown in Figure 2, some improvement to the characteristics of the level meter has been adopted in the design of the optical system and the electronic circuitry of the level meter. The complementary characteristics of the infrared level meters and the gyro have been fully utilized in this measurement system. The gyro output has a small high frequency noise but also a significant constant drift. Hence, it cannot be used as a long term standard of measurement by itself while the infrared level meter has a small constant drift. Thus it is usable as a long term standard for measurement, but it has significant alternating noise. It cannot give the measurement standard for the yaw altitude and cannot be used by itself. By combining these two elements, they will complement each other and form a better attitude measurement system.

From Figure 2, it can be seen that the long term measurement standard of this measurement system is provided by the infrared level, and the transient measurement standard is provided by the gyro with three channels of relatively smooth attitude deviation signals

provided by the gyro. Namely, the pitch deviation signal is provided by the small feedback loop of the infrared pitch level meter and the horizontal gyro, the yaw and roll deviation signals by the infrared roll level meter and the vertical gyro as the gyro compass. The programming mechanism on the axis of the outer frame of the horizontal gyro is used to establish the programmed attitude deviation signals

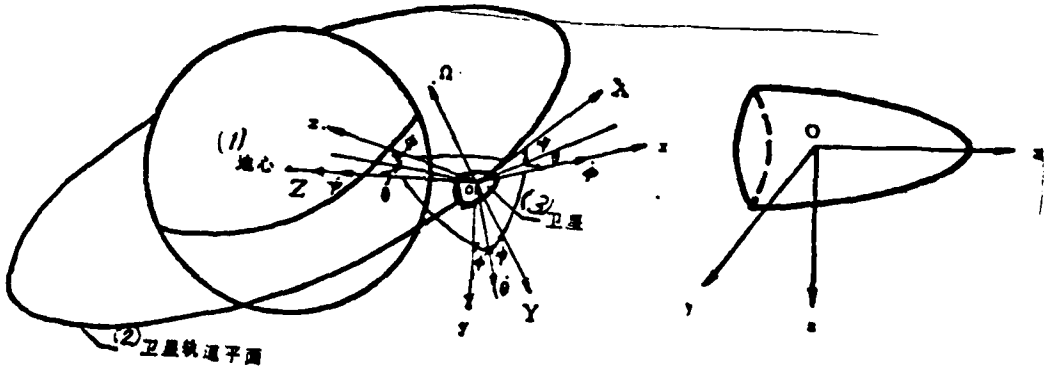

Figure 1. The coordinate systems and their relationship. OXYZ is the Earth-centered orbital coordinate system. oxyz is the satellite coordinate system.

1- center of Earth; 2- satellite orbital plane; 3- satellite

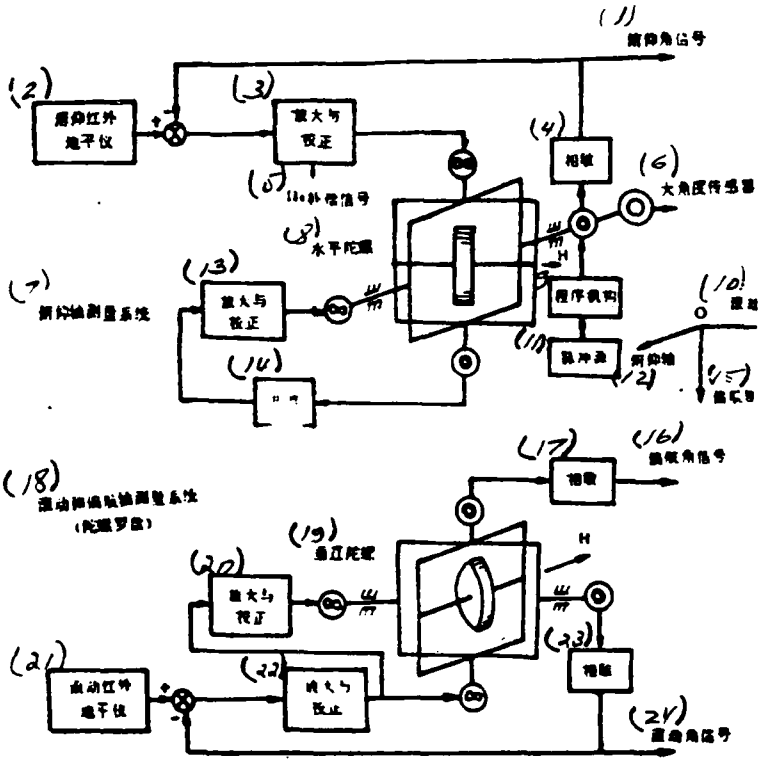

Figure 2. Schematic of the attitude measurement system composition.
●— transducer ●— force coupling device

1--pitch angle signal; 2--pitch infrared levelmeter; 3--amplification and correction; 4--phase sensor; 5--compensation signal; 6--large angle transducer; 7--pitch axis measuring system; 8--horizontal gyro; 9--programmed mechanism; 10--roll axis; 11--pulse source; 12--pitch axis; 13--amplification and correction; 14--phase sensor; 15--yaw axis; 16--yaw angle signal; 17--phase sensor; 18--roll and yaw axis measuring system (gyro compass); 19--vertical gyro; 20--amplification and correction; 21--roll infrared levelmeter; 22--amplification and correction; 23--phase sensor; 24--roll angle signal

during the establishment of the return attitude. The large angle transducer may be used to monitor the working condition of the attitude control system during the establishment of the return attitude. In eliminating the initial attitude deviation as well as in establishing the return attitude, the infrared level must be cut off from the attitude measurement system so that the system is in an open circuit measurement mode, i.e., the two gyros are both situated in a free gyro state. Figure 2 shows the working status of the measurement system in orbit.

When the orbit is nearly circular, Figure 2 may be simplified to the block diagram as shown in Figure 3 within the linear operational range of small signals.

From Figure 3, we can write the following equations:

$$\frac{d}{dt}(\theta_G-\theta)=K_\theta(\theta_H-\theta_G)+\Omega_o-\Omega+D_2 \qquad (1)$$

$$\frac{d}{dt}(\psi_G-\psi)+\Omega(\phi_G-\phi)=K_\psi(\phi_H-\phi_G)+D_3 \qquad (2)$$

$$\frac{d}{dt}(\phi_G-\phi)-\Omega(\psi_G-\psi)=K_\phi(\phi_H-\phi_G)+D_1 \qquad (3)$$

where θ, ψ and ϕ are the pitch, yaw and roll attitude angles of the satellite. θ_G, ψ_G and ϕ_G are the pitch, yaw and roll frame angles of the gyro. K_θ, K_ψ and K_ϕ are the amplifications on the gyro advancing angular velocities provided by the amplifier and the gyro coupling device. D_1, D_2 and D_3 are the equivalent drift velocities of the gyro along the roll, pitch and yaw axes, including the components and quadratic coupling terms along the corresponding axes of the gyro drift velocity, the orbital plane advancing angular velocities, etc., Ω and Ω_o are respectively the instantaneous and normalized orbital angular velocities, the latter being provided by the amplifier. Both Figure 3 and equations (1), (2) and (3) indicate that the critical parameters here are K_θ, K_ψ and K_ϕ. The principle of their selection

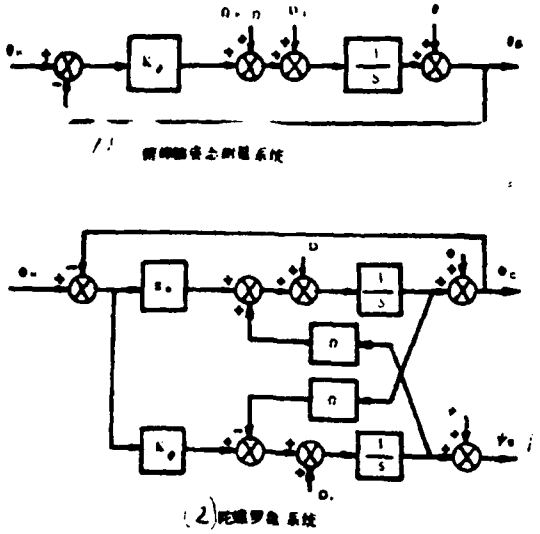

Figure 3. Simplified block diagram of the attitude measuring system.
1--pitch axis attitude measuring system; 2--the gyro compass system

should be based upon the noise of the levelmeter and the drift rate of the gyro on the corresponding axes, so as to minimize the mean square value of the attitude measurement error. At the same time, consideration must be given to the effect of the noise of the levelmeter on the rate of gas consumption produced through the central circuit. This is important to satellites of medium and low orbits, especially when infrared levelmeter wavelength cannot be located in the idealized 14-16 micron band. In the design of this system, we considered the maximum drift rate of the gyro is 4° per hour, the mean square value of the infrared levelmeter error is 0.25°, 1000 times the bandwidth for the steady noise for the orbital angular velocity. The value range of the three parameters mentioned above is determined under these conditions.

The following problems should also be considered in the system design:

(1) Limiting the maximum saturated advancing angular velocity of the gyro: To avoid the increase of the attitude deviation and excessive system gas usage rate produced by the high output signals when the levelmeter scans the sun or the moon during normal flight of the satellite, the range of values of K_θ, K_ψ and K_ϕ should be limited. In our system design, we require that:

the saturated pitch advancing angular velocity $\leqslant$ = 0.06%
the saturated yaw advancing angular velocity $\leqslant$ = 0.054%
the saturated roll advancing angular velocity $\leqslant$ = 0.018%

(2) The problem of matching the transmission coefficients of the infrared levelmeter and the gyro: During technical implementation, the transmission coefficient K_h between the input angle and output potential of the infrared levelmeter may deviate from the transmission coefficient K_g between the input angle of the gyro and the transducer output potential. Analysis and experiment demonstrate that when K_h is different from K_g, the system will be induced to operate in a limiting loop of multiple gas propulsion, thus increasing the gas consumption rate. The effect on the roll channel is more pronounced than the other two channels. For example, when K_h is larger than K_g by 10%, the yaw mini-propulsion system undergoes a steady "double propulsion phenomenon". The limiting loop angular velocity and the gas consumption rate both double. In our design, we require

roll channel $(K_h - K_g)/K_g \leqslant = 6\%$
yaw and pitch channel $(K_h - K_g)/K_g < = 10\%$

(3) Selection of the gyro phase sensitivity time constant T_g. Apparently the increase of T_g will decrease the resistance of the system. When T_g reaches a certain value, the joint operation of the large and small propulsions of the system may be damaged. The dynamic characteristics of the pseudovelocity increment feedback system indicatethat T_g is not greater than its recharge time constant T_{fc}. In general, we should let $T_g \leqslant = 0.2$.

(4) The time constant T_h of the infrared levelmeter: The increase of T_h will induce the steady state limiting loop operating

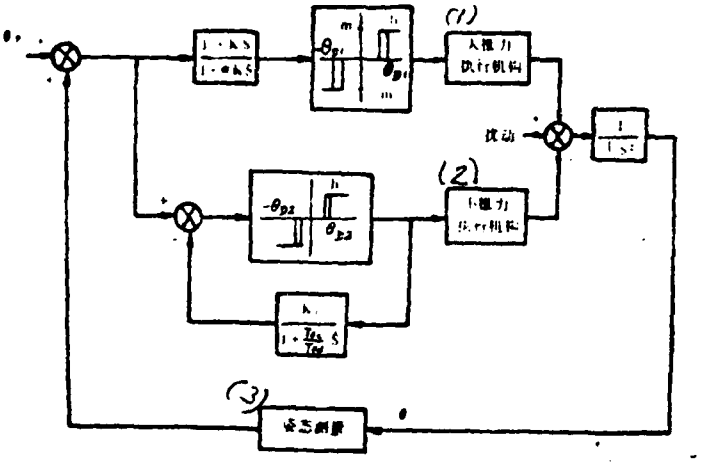

Figure 4. Flow chart of the pitch channel control system
I = satellite pitch axis rotational inertia
S = Laplacian
1--high powered execution mechanism; 2--low powered execution mechanism; 3--attitude measurement

speed and the gas usage rate to increase. It is best to have T_h smaller than the time constant of the tracking miniloop of the measurement system by one order of magnitude. Generally, we should let T_h < 2 seconds.

2. The central control circuit and the execution mechanism

In order for the system to accomplish its tasks well in the three different working stages, as well as to be simple, reliable, light in weight and economic in power consumption, we adopted two types of switch-controlled cold-gas propulsion mechanisms, one with a high power and the other a low power. Figure 4 is the flow chart of the pitch channel control system. Figure 5 is the chart of the organizational principle of the execution mechanism.

For convenience, we shall use the pitch channel as an example to describe the high and low power propulsion systems, and we shall consider the external frame angle of the horizontal gyro of the measurement system as approximately the pitch attitude angle of the satellite.

(1) The high power propulsion leading correction system: The high powered propulsion leading correction system is mainly used to eliminate the satellite's initial attitude deviation stage and to establish quickly the re-entry attitude stage. In order to increase the resistance of the system, a leading correction network is adopted. The principle requirement in the design of a high powered propulsion system is to eliminate the initial attitude deviation with a minimal amount of gas usage and to establish the attitude needed for the re-entry of the satellite with the shortest amount of time and the minimal amount of gas.

From Figure 4, it can be seen that under the condition that the dynamic characteristics of the execution mechanism and the effect of the time constant αK of the leading correction network are ignored, the law of control of the high powered propulsion system may be described with the following equations:

$$m=-1,\ mA=-A,$$
$$\theta+\theta_p+K(\dot{\theta}+\dot{\theta}_p)\geq\theta_D \quad (4)$$
$$m=+1,\ mA=+A,$$
$$\theta+\theta_p+K(\dot{\theta}+\dot{\theta}_p)\leq-\theta_D \quad (5)$$
$$m=0,\ mA=0,\ \text{当}-(1-h)\theta_D\leq\theta+\theta_p+K(\dot{\theta}+\dot{\theta}_p)\leq(1-h)\theta_D \quad (6)$$
$$\ddot{\theta}=A_d+mA=(M_d+mFl_j)/I \quad (7)$$

Here θ_p and $\dot{\theta}_p$ are respectively program turn angle and angular speed in establishing the re-entry altitude. A_d and A are respectively the angular acceleration produced by the force moment of the disturbance M_d and the control force moment Fl_j, F is the propulsion force, l_j is the lever. Apparently, during the period of eliminating the initial altitude deviation, θ_p and $\dot{\theta}_p$ are both 0. In practical design, in order to take into consideration the effects of the dynamic characteristics of the execution mechanism and of the time constant K, equations (4)-(7) should be modified. We shall briefly describe the problems of selecting the principal parameters contained in the above equations.

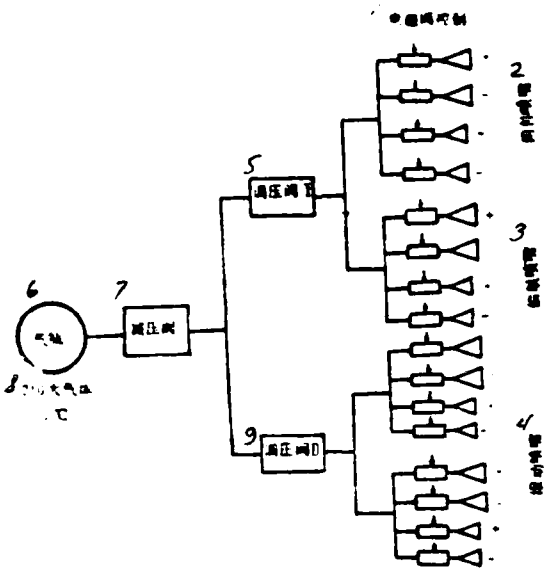

Figure 5. Organizational principle of gas propulsion execution mechanism

1--electromagnetic gate control; 2--pitch jet; 3--yaw jet; 3--roll jet; 5--pressure adjustment gate; 6--gas bottle; 7--pressure reduction gate; 8--210 atmosphere 0°C; 9--pressure adjustment gate

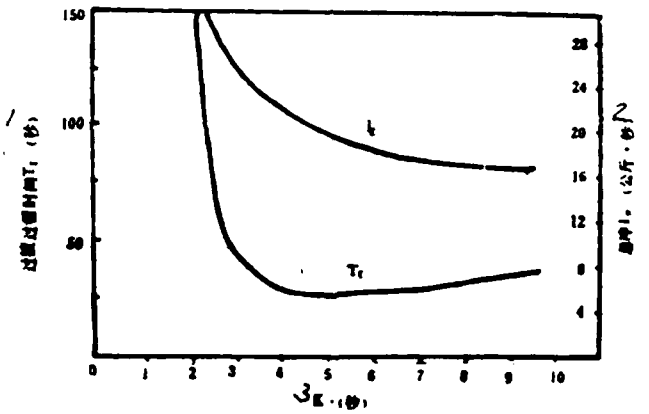

Figure 6. Curves of the transition time T_t and total propulsion momentum I_Σ vs. K.

1--transient period time T_t(sec); 2--total impulse I_Σ (kg/s) 3--K (s)

i) selection of the leading correction network parameter K: Under the above mentioned simplified conditions, the effect of parameter K on the transition period time T_t and on the total propulsion momentum I_Σ may be plotted by using either the analytical method of the simulation method as shown in Figure 6. T_t is the time needed to eliminate a certain amount of initial attitude deviation. After

the relative impulse of the gas is given, the gas consumption rate Q may be found from the total impulse I_Σ by proportion. In establishing the re-entry attitude, it corresponds to the time needed to eliminate the satellite attitude angular deviation and the attitude angular velocity after the pitch axis has turned to a pre-determined angle θ_p according to program. Figure 6 shows that under the condition that the other parameters are relatively fixed, T_t and I decrease with K within a certain range, but when K is greater than four seconds, T_t even increases slightly. Hence, it is suitable to choose K = 4 secs.

ii) Selection of the switching characteristic dead region and the stagnant ring coefficient: In order to save gas, the high powered propulsion system will not be used if the attitude deviation is within ±1°. At the same time, it is not suitable to select too big an θ_D if we want to make the satellite pitch attitude rapidly reach $\theta_p + \varepsilon$ (where ε is the allowed error). In our design, we take $\theta_D = 1°$. When the stagnant ring coefficient h is large, the noise suppression ability is high but the system stability is not good. After synthetic consideration, we take h = 0.1.

iii) Selection of the control of angular acceleration A: When the effect of A on T_1 and I_Σ is considered, we can draw Figures 7 and 8. From the graphs one can see that at K = 3-6 sec, when $A > 0.5°/s^2$, both T_1 and I_Σ fail to decrease with increasing A. When A is too small, T_1 and I_Σ increase significantly. Hence, it is suitable to select $A = 0.5°/s^2$. 6

iv) Selection of programmed turn velocity $\dot{\theta}_p$: For simplicity, reliability and ease of implementation, we have chosen to use fixed programmed turn velocity $\dot{\theta}_p$. The selection of $\dot{\theta}_p$ should be balanced between T_R (time needed to establish re-entry attitude) and the gas consumption rate Q. Here we try to minimize Q under the condition that $T_R \leq$ = 60 sec. In the design, we chose $\dot{\theta}_p \approx 2.67 \times 10^{-2}\theta_p°/s$.

(2) Low powered propulsion system: The low powered propulsion system is used chiefly in situations which requires highly precise

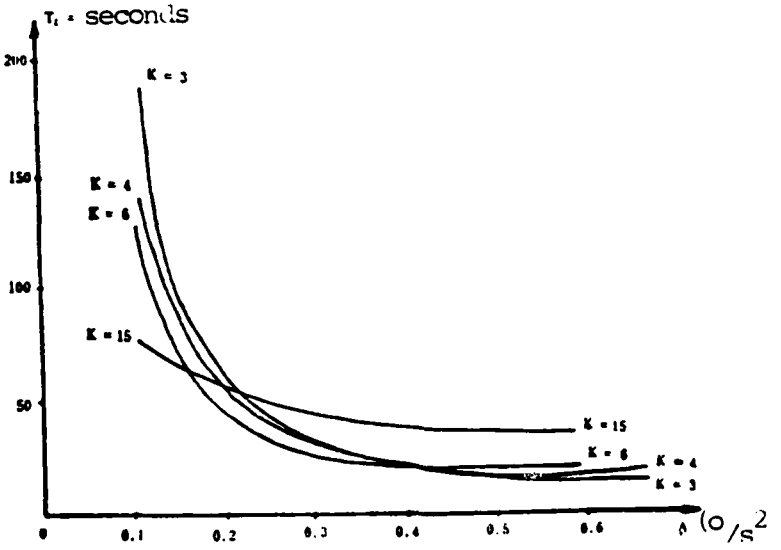

Figure 7. Relation of transition time T_i and control angular acceleration A

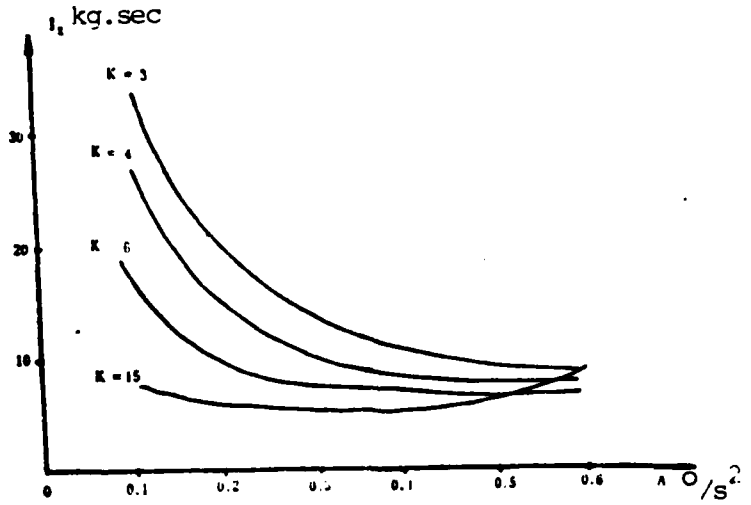

Figure 8. Relation of total propulsion momentum I_Σ and angular acceleration

attitude control over long periods of orbital motion. In order to minimize the amount of gas usage needed to satisfy the required attitude precision and attitude angular velocity with good dynamic resistance and long life, we adopted a pseudo-velocity increment feedback control system with the discharge time constant T_{fd} greater than the charging time constant T_{fc}, as shown in Figure 4.

The pseudo-velocity increment feedback control system is a pulse regulated system. Under the situation of no disturbing force moment, the system is in an ideal limiting cycle (1) operational state as shown in Figure 9(a) (when no speical measure is taken, it is very difficult for the system to operate in the optimal limiting cycle (2) operational state). The equivalent minimal propulsion pulse width T_d output by the system is

$$T_d = T_{on} + \Delta T \tag{8}$$

$$T_{on} = -T_{fc} \ln\left(1 - \frac{h\theta_d}{K_{fa}}\right) \tag{9}$$

$$\Delta T = (T_{pd} - T_{pr}) + (T_{md} - T_{mr}) \tag{10}$$

where T_{on} is the minimal pulse width from the pseudo velocity increment controller, ΔT is the increased pulse width after the pulse delay is taken into consideration. It is determined by equation (10) where T_{pr} and T_{pd} are respectively the leading and trailing delay time of the electromagnetic gate. T_{mr} and T_{md} are respectively the leading and trailing edge equivalent time constants of the propulsion jet. θ_d is the stagnant region of the pseudo-velocity increment controller. Here the limiting cycle angular velocity is

$$\theta_B = \frac{a}{2} T_d = -\frac{aT_{fc}}{2} \ln\left(1 - \frac{h\theta_d}{K_{fa}}\right) + \frac{a\Delta T}{2} \tag{11}$$

Under the condition that the ratio of the satellite structure to the jet gas volume is constant, we may define the unit time angular velocity increment to be the weighting factor of the gas usage, denoted as q; then during the ideal limiting cycle operational periods with no disturbing force moment,

$$q = \frac{2a}{T} T_d = \frac{\theta_B}{\theta_d} = \frac{f^2 I_j^2}{4l^2 \theta_d} T_j \tag{12}$$

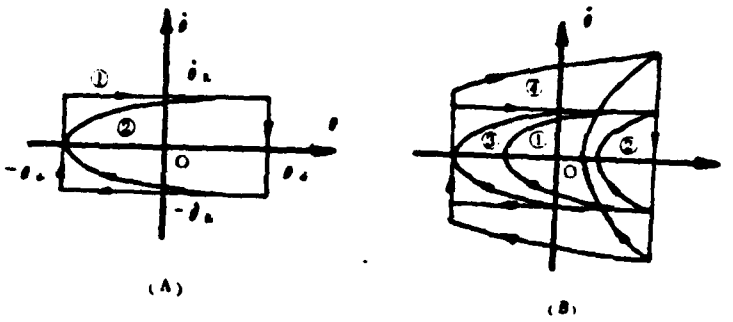

Figure 9. The limit cycle operation of the pseudo-velocity increment feedback system.

Here a is the control angular acceleration produced by the action of the small propulsion f. T is the period of the limit cycle. It can be seen from equations (11) and (12) that to decrease $\dot{\theta}_R$ and lower q, we need to decrease T_d, and the smaller ΔT is, the better. But in reality, ΔT is generally greater than zero, hence T_d is generally greater than T_{on}.

However, under the action of force moments, the system is in the limit cycle (1) and (2) operational state as shown in Figure 9(b). Under most circumstances, it is difficult to be in the optimal limit cycle (3) operational state. Here curve (1) is the phase trajectory when the disturbing force moment is less than that for curve (2). Apparently, the smaller $\dot{\theta}_R$ is designed, the easier it is to cause propulsion on one side. The bigger the disturbing force moment, the more frequent will be the propulsion. If the impulse moment ΔH_b produced on the satellite by the disturbing force moment H_d is constant, then theoretically speaking, the mass of the gas used to overcome the disturbing force moment will also be constant. If the jet used each time is completely utilized to overcome the disturbing force moment, then the number of propulsions is

$$\eta = \frac{\int M_d dt}{Fl_1 T_d} = \frac{\Delta H_d}{Fl_1 T_d} \qquad (13)$$

From equation (13) it can be seen that when a disturbing force moment exists, in order to reduce the number of times the electromagnetic gate operates, to increase the life of the execution mechanism

and not to increase the gas usage, then one should suitably increase $\dot{\theta}_R$ or T_{on} with the condition that the attitude angular velocity for fixed direction Earth-oriented observation should be satisfied. It should be noticed that it is not good to increase T_{on} suitably. Then propulsion from both sides will again occur (see Figure 9(b) curve 4), causing the gas usage rate to decrease which is not desirable.

In summary, for the yaw channel which has a large constant disturbing force moment, we have made in our design its limit cycle velocity about twice that of the pitch and roll channels which have the smaller constant disturbing force moment. The corresponding T_d satisfies the same kind of relationship. $\dot{\theta}_R$ and T_d are selected as shown in Table 1.

Table 1. Results of $\dot{\theta}_R$ and T_d selection

parameter / channel	parameter limit cycle angular velocity $\dot{\theta}$	equivalent minimum propulsion pulse width T_d
pitch and roll	2.5×10^{-3} o/s	50 ms
yaws	5.0×10^{-3} o/s	100 ms

Table 2. Distribution of T_{on} and ΔT

parameter / channel	T_{on} (ms)	ΔT (ms)
pitch and roll	37	13
yaw	67	13

It may be seen from equation (11) that $\dot{\theta}_R$ is determined by T_d. In selecting $\dot{\theta}_R$ and T_d, we should consider the problem of selecting a. In the design we have chosen a = 0.1 $^o/s^2$. It is much greater than the angular velocity produced by the disturbing force moment, hence making sure that the high and low powered propulsions will operate in conjunction. At the same time, a is not too small so that it is easily implemented.

In addition, we may suitably distribute T_{on} and ΔT from equation (8) in accordance with necessary analysis and experimentation. In our design, the distribution of T_{on} and ΔT is shown in Figure 2.

As is well known, as far as pseudo-velocity increment feedback control system is concerned, when the attitude deviation θ reaches a certain value θ_s, the system will be in a continuous propulsion state. We call the attitude deviation θ_s which starts such a state by the name "saturated jet angle". It may be expressed as

$$\theta_s = K_f \alpha + (1-h)\theta_d \qquad (14)$$

8

It is an important parameter to guarantee that the high and low powered propulsions operate in conjunction. In our design, we have considered the fact that the high powered propulsion switch characteristic stagnant region θ_D is 1°. To guarantee that the high and low powered propulsions do operate in conjunction, we took θ_s to be 0.6-0.75°.

Besides, under the condition that the operational characteristics of the execution mechanism and that of the measurement system are not considered, the system may be roughly seen as a second order linear system with resistance ratio ζ and natural frequency ω_n by the descriptive function method.

$$\zeta = \sqrt{\frac{T_{1c} T_{1d}}{4K_1}} \qquad (15)$$

$$\omega_n = \sqrt{\frac{T_{1c}}{T_{1d} K_1}} \qquad (16)$$

After the basic relationship and data are given as above, we can then proceed to make selections on some of the other major parameters of the low powered propulsion system without much difficulty.

i) Selection of the switching characteristics: The stagnant region θ_d should match the measurement error of the measurement system in order to satisfy the attitude precision requirement of the orbital motion while the switch stagnant region of the low powered

propulsion system θ_d should be much smaller than that of the high powered propulsion system θ_D so that the low powered system is the one that operates in the orbital motion. We chose $\theta_d = 0.3°$.

Stagnant cycle coefficient h affects T_{on} on one hand, while it also affects to a certain extent the ability of the system to suppress noise. From equation (9), we know that when the other parameters are held constant, the smaller h is, the smaller T_{on} will be, while the ability to suppress noise will be weaker. Taking into consideration that the selection of the other parameters has already provided the system with a strong noise suppression capability, we chose h = 0.1 after some simulation testing and analysis.

ii) Selection of the feedback network parameter: In order to make sure that the high and low powered propulsion work in conjunction, we take $\theta_s = 0.7$. From equation (14), it may be determined that $K_f = 4.3$ secs.

In order to make sure that the pulse width T_{on} is minimal, we may compute from equation (9) the charging time constant T_{fc} based on the other parameters already determined. In order to make sure that the system possesses a large resistance, we can determine the discharging time constant T_{fd} from equation (15). In the design, we take $\zeta = 1$. Thus, the results of selecting T_{fc} and T_{fd} are shown in Table 3.

The results of the selection of the principal parameters for the high and low powered propulsion systems may easily be transformed into the requirements on the dynamic characteristics and the size of power of the propulsion execution mechanism. The normalized values of the high and low propulsion strengths of the various channels are shown in Table 4.

In the preliminary system design stage, a large amount of mathematical simulation experimentation was carried out. After the initial production samples were produced, experiments with the real and semi-real objects were done to verify the system design. The joint exerti

Table 3. Results on the selection of T_{fc} and T_{fd}

parameter / channel	charging time constant T_{fc} (μs)	discharging time constant t_{fd} (sec)
pitch and roll	510	30
yaw	900	30

Table 4. Normalized values of the propulsion strength for all channels

type / channel	high power (gm)	low power (gm)
pitch	1000	200
yaw	1000	200
roll	350	70

of the high and low powered propulsion in each channel and the effect on the coupling of the three axes are also studied. Based on that study, the prototype was developed. The interface relationship between the main system and its various sub-systems and the requirements of them were then finalized. In the development of the prototype, a large amount of analysis and experimentation was carried out to satisfy the reliability required for the satellite after launch. We shall not describe them owing to the limitation of space.

III. RESULTS OF FLIGHT TESTS

In order to examine the operational characteristics of the attitude control system in the flight test and to obtain some useful data, stellar cameras that are capable of discriminating the precision of the attitude control system are installed in the satellite besides setting up some remote sensing parameters related to the attitude control system. We shall briefly describe below the operational status and preliminary analytical results of the attitude control system in three different operational stages according to the data obtained in the three flight tests.

1. The stage during which the initial attitude deviation is being eliminated.

Remote data indicate that among the three satellites, the first one launched had a relative bad initial attitude deviation. The two satellites launched later had made great improvement. With the first satellite as an example, Table 5 shows its initial attitude deviations. The dynamic procedure to eliminate the initial attitude deviation is shown in Figure 10.

Table 5. The initial attitude deviation of the first satellite

attitude deviation / channel	initial attitude angle(degree)	initial attitude angular velocity ($^\circ/_s$)
pitch	+1.13°	-2.24
yaw	+1.68°	+0.17
roll	+0.98°	-0.17

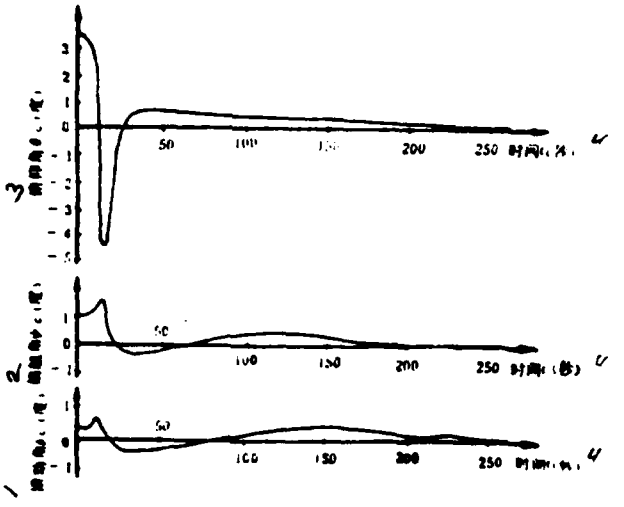

Figure 10. Dynamic process in the elimination of the initial attitude deviation for the first satellite. (from remote gyro data).
1--roll angle; 2--yaw angle; 3--pitch angle; 4--time (sec)

The operational properties of the attitude control system may be seen from Table 6.

TABLE 6

content / satellite no.	max. angle of adjustment or procedure characteristic point	time on entering 0.7°
I	-5.36°	12 sec
II	single adjustment decay	12 sec
III	single adjustment decay	6 sec

The above situation indicates that the operation of the attitude control system during the initial attitude deviation elimination stage is normal and is very close to the theoretical analysis. The system has a strong initial attitude capture capability.

2. During the orbiting stage

(1) Concerning the accuracy of the attitude control. The actual accuracy attained by the attitude control system is obtained according to the stellar camera data. The stellar camera obtains first the attitude angle of the satellite relative to the Earth-centered astronomical coordinate system by using the method of photographing the stellar sky, and then transforms it into the attitude angle relative to the Earth-centered orbital coordinate system from the orbit tracking data. The satellite attitude obtained from the stellar camera data is more accurate. Figure 11 shows the typical attitude data obtained from the stellar camera data. The attitude angle and attitude angular velocity deviation actually attained are displayed in Figure 7.

TABLE 7. Attitude deviation actually attained

content / channel	attitude angle deviation	attitude angular deviation
pitch	$\leqslant = 0.7$	$\leqslant = 0.01$
roll	$\leqslant = 0.7$	$\leqslant = 0.02$
yaw	$\leqslant = 1.5$	$\leqslant = 0.02$

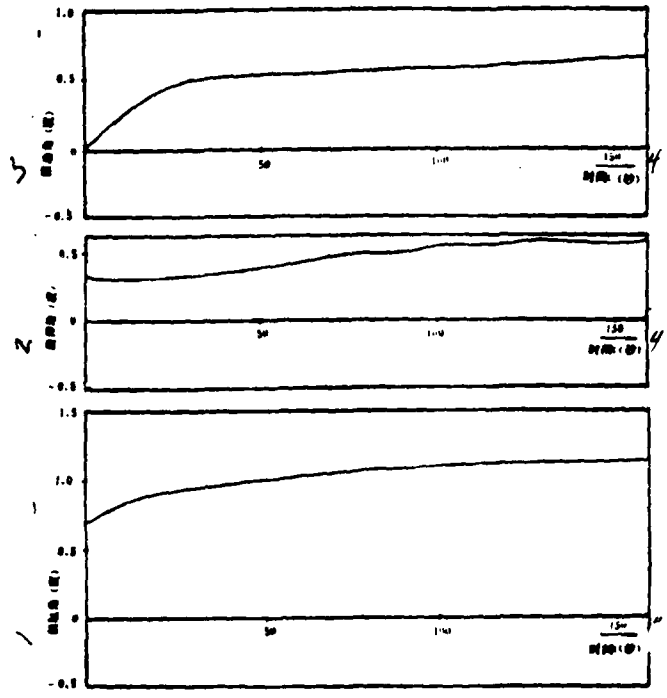

Figure 11. Typical attitude data from stellar camera 1--yaw angle; 2--pitch angle; 3--roll angle; 4--time (sec)

(2) Concerning the spectral density of the infrared levelmeter noise: Preliminary analysis has been carried out on the infrared levelmeter output noise based on the remote data on the infrared levelmeter and the gyro frame angle during the oribtal motion stage. In the analysis, a smooth random model is assumed for the noise. The power spectral density of the infrared levelmeter output noise then can be calculated through Fourier transform. We used a method similar to that in [4]. After making a dynamic correction on the measuring system, it is found that the band width of infrared levelmeter output noise power spectral density is approximately 12 times the orbital angular velocity. Because there is not enough continuous, analysable data, this is only a preliminary result usable for reference.

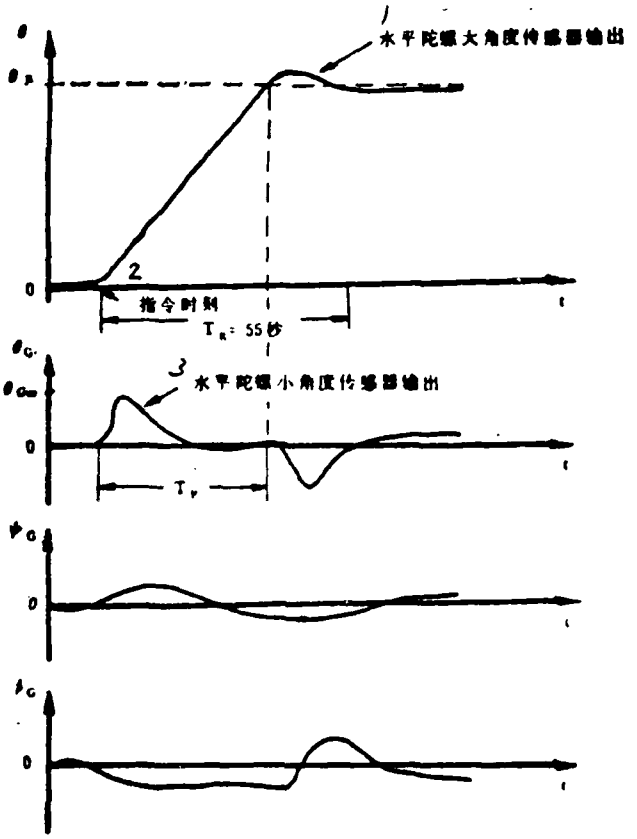

Figure 12. Typical operational character in establishing re-entry attitude (obtained from gyro remote data)
1--output from horizontal gyro large angle transducer; 2--command time; 3--output from horizontal gyro small angle transducer

3. During the stage of establishing re-entry attitude

During the re-entry attitude establishment stage, the attitude control basically operates in the same way in the three satellites. Its typical operational character is shown in Figure 12. It shows the complete dynamic process in establishing re-entry attitude by the attitude control system of the third satellite.

From Figure 12, it may be seen that

(1) the output from the horizontal gyro's outer frame large angle transducer indicates that the satellite had rotated about the

pitch axis in the negative direction through an angle θ_p degrees. Its dynamic process agrees exactly with the theoretical analysis.

(2) The output from the horizontal gyro's outer frame small angle transducer indicates that at the beginning of attitude adjustment, the output rises sharply with a positive sign to reach a maximum over-adjustment angle. After a certain time period T_p, the output is almost zero. It can be ascertained from this process that the program mechanism turns through θ_p degrees with speed $\dot{\theta}_p$ according to a pre-determined program in a pre-determined direction. The satellite will also attain this angular velocity. Finally, the satellite is stabilized in the range $\theta_p + \varepsilon$. The complete attitude adjustment process takes about 55 seconds.

The above indicates that the process of establishing re-entry attitude basically agrees with the prediction. The operation is entirely normal.

4. Concerning the gas usage rate of the attitude control system

The experimental results of three flights indicate that the gas usage rate of the attitude control system (whether theoretical estimate or actual consumption) gradually decreased, especially for the third satellite. Its gas consumption is two times smaller than that of the first satellite. The main reasons for this decrease are:

(1) based on the experiment of the first two flights, we have modified the parameters of the attitude control system of the third satellite, especially the principal parameters of the measuring system. We have also improved the noise suppression ability of the system and reduced gas consumption rate.

(2) we have added a front filter to the infrared levelmeter optical system, improved the bandwidth of the meter and reduced the effect of the sun, the moon and the cold cloud on the output of the infrared levelmeter, hence reduced the gas consumption.

IV. CONCLUSIONS

The results of the three flight tests indicate that the planning and design of the satellite attitude control system of our first generation re-entry type Earth-oriented fixed direction observation technique is correct. The system worked reliably and operated normally. In particular, the improvement on the third satellite is effective. The mission is completed satisfactorily and some useful data have been obtained. Some experience has been accumulated which has established a foundation for developing similar satellite control systems in the future.

In the future, it is necessary to improve on the accuracy of the attitude control system, especially the yaw attitude accuracy. The operational lifetime of the satellite should be lengthened with reduced development budget. System engineering and modern control theory should be applied well to the design and development of attitude control systems.

REFERENCES

[1] Yang Jiachi, Zhang Guofu, Sun Chengqi, "Three Axis Stabilized Attitude Control System for Chinese Near Earth Orbit Satellites," VIII IFAC Symposium on Automatic Control in Space, Oxford, UK. 2-6 July, 1979.

[2] Bowers, J.L., Rodden, J.J., Scott, E.D. and DeBra, D.B., "Orbital Gyrocompassing Heading Reference," *J. Spacecraft and Rockets*. Vol.5, p. 903, 1968.

[3] Bryson, Jr., A.E. and Kortum, W., "Estimation of the Local Attitude of Orbiting Spacecraft," *Automatica*, Vol.7, pp 167-180, 1971.

[4] Weiss, R., "Conical Scan CO_2 Horizon Sensing Orbit Accuracy and Horizon Noise Model," AIAA Guidance, Control and Flight Mechanics Conference, Vol.2, Aug. 17-19, 1970.

[5] Jerry, M. Mendel, "Performance Cost Function for a Reation-Jet Controlled System During on On-off Limit Cycle," IEEE Trans. on Automatic Control, Vol. AC-13, pp. 362-368, 1968.

[6] Jerry, M. Mendel, "On-off Limit Cycle Controllers for Reaction-Jet Controlled Systems," IEEE Trans. on Automatic Control, Vol. AC-15, No.3, 1970.

[7] Scott, E.D., "Pseudo-rate Sawtooth-pulse-rest Control System Analysis and Design," *J. Spacecraft and Rockets*. Vol. 4, p. 781, 1970.

GUIDANCE ACCURACY DETERMINATION BASED ON DATA MEASURED EXTERNALLY DURING PROPULSION-FREE STAGE

Zhu Wenxuan

ABSTRACT

We propose in this paper to measure the position vector of a space vehicle in its propulsion-free orbit with radar and compare it with the normalized oribtal position vector. By treating the difference variationally with matrix theory, it is possible to determine the total guidance aberration of the guidance system instruments on the space vehicle when the thrust ends. This may provide an auxiliary method for accuracy checking to compensate for the shortcomings of the ballistic measurement devices during propulsion as well as the accurate position vector of the normalized orbit during atmosphere re-entry.

I. INTRODUCTION

The accuracy of the guidance system and inertial system of carrier rocket-type space vehicles, especially the accuracy in the measurement of inertial instruments, is a problem of common concern for departments designing, testing and using space vehicles. One of the important goals of developing highly accurate remote measurement systems and large, complex and highly accurate ballistic measurement systems is to determine the accuracy of the guidance system and its inertial sensitivity measurement instruments, as well as to determine the reliability of the ground test accuracy of the inertial instruments.

When the space vehicle is under propulsion (engine thrust), there exist large acceleration and sudden impulse, random and large rotations about the center, complex and severe vibrations of the three axes, large variations in pressure and temperature as well as all kinds of radiation interference. For inertial instruments working in this kind of environment under conditions far worse than those in

the laboratory or ground level factory, it is necessary to use vehicle ballistic measurement parameters one order of magnitude more accurate than those measured by the inertial instruments to compare with the internal remote measurement parameters, and to treat and analyze the huge amount of accurate, reliable data in order to obtain reliable results in determining the operational accuracy, in measuring the sensitivity and in varying the parameters being measured. However, for certain types of vehicles, it is often impossible to realize the required accuracy due to limitations in material conditions and measurement accuracy.

In the known gravitational field of the Earth, satellite type vehicles move in thrustless free flight state. By tracking these vehicles with ballistic measurement systems and measuring their orbital parameters as well as analyzing and carrying out computational treatments on the measured data, it is possible to obtain a synthetic determination, including both propelled and propulsion free flights) for the total guidance accuracy of the inertial system, and to compensate for the shortcomings in determining the accuracy of the inertial system in the propelled stage. In this paper we shall discuss the theoretical aspect of this method.

II. THE BASIC PRINCIPLES

To determine the orbit of a space vehicle with the externally measured parameters of the propulsion-free (0 thrust) vehicle is a common method used by departments designing, testing and utilizing the vehicle. Using these externally measured parameters to determine the total guidance aberration (accuracy) is a new direction in using these parameters.

After the thrust on the vehicle has ended (engine shut-off), the velocity of the vehicle may reach thousands of meters per second at a height of more than 100 kilometers. Over most of the flight time, the atmosphere in the orbit is very rare so that aerodynamics may be neglected. In comparison with the gravity of the Earth, one

may also neglect the effect of photon pressure, radiation pressure and gravitational attraction of other heavenly bodies on the vehicle. Hence, the vehicle travels along a pseudoelliptic orbit solely under the Earth's gravitational attraction (if we regard the Earth as a sphere and not a spheroid, i.e., we neglect the oblateness of the Earth, then the gravitational force is an inverse square, central force. The vehicle will move in a plane along a pseudoelliptical orbit). The principal parameters of this pseudoellipse such as the semi-major axis and eccentricity are uniquely determined by the velocity $\vec{v}'(V_x,V_y,V_z)$ and position $\vec{r}'(x,y,z)$ when the thrust is ended. The pseudoellipse of satellites and spacecraft does not intersect with the Earth. They will rotate around the Earth. The pseudoellipse of a guided missile and its warhead does intersect with the Earth. It has to re-enter the atmosphere and fall in a pre-determined target region. The positions of at least three points, $\vec{r}_1(x_1,y_1,z_1)$, on the orbit of the vehicle in a propulsion-free region, should be measured if one uses external ballistic position measurement systems, such as single pulsed radar or photographic theodolites with lower accuracy than that used in propelled flight. The angle subtended by each pair of points should be greater than $0.5 \sim 1°$. The true pseudoelliptic orbit of the vehicle may then be obtained by applying proper computations on $\vec{\gamma}_3$. This is then the ordinary orbit determination method. 24

The velocity $\vec{v}'$ and position $\vec{r}'_0$ at the thrust termination point (engine shut-off point) may also be derived through proper computations from the $\vec{\gamma}_3$ on two points which subtend an angle at the center of the Earth greater than $0.5 \sim 1°$. The combination of $\vec{v}', \vec{r}'$ is needed to satisfy the guidance condition or for the guidance system to fulfill its mission. Their deviation from the theoretically computed velocity $\vec{v}'_0$ and position at $\vec{r}'_0$ at t^f when the thrust stops:

$$\begin{aligned} \delta\vec{v}' &= \vec{v}' - \vec{v}'_0 \\ \delta\vec{r}' &= \vec{r}' - \vec{r}'_0 \end{aligned} \tag{2-1}$$

are the basic data for calculating the total guidance error. The deviation from the target of the missile impact point calculated from

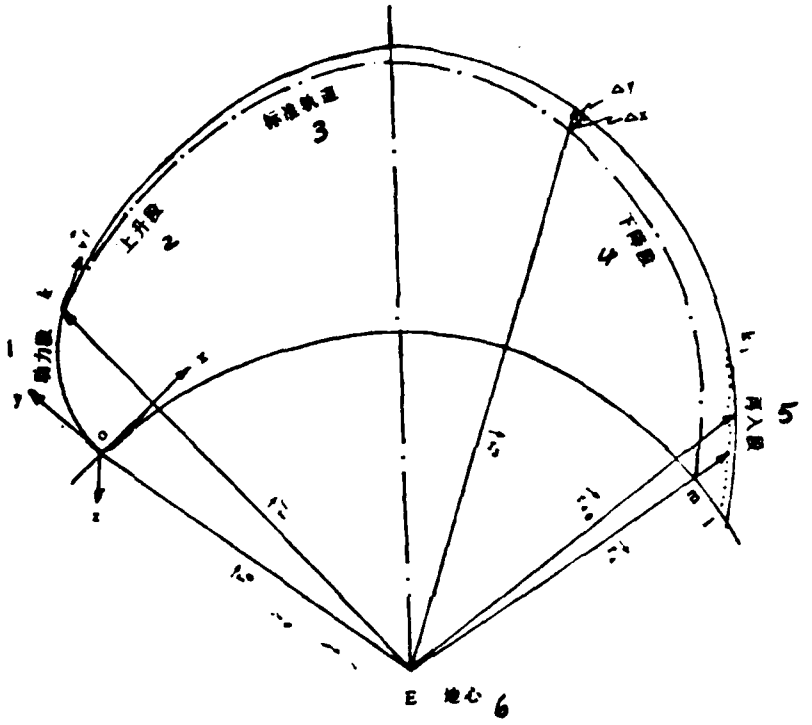

1--propelled stage; 2--ascending stage; 3--standard orbit;
4--descending stage; 5--re-entry stage; 6--center of Earth

24

$\delta\vec{v}'$ and $\delta\vec{r}'$ (off-target amount) and the deviation of the number oribts of the satellite or spacecraft all belong to the total guidance error. After reducing from $\delta\vec{i}$, $\delta\vec{r}$, , the errors $\delta\vec{v}'$, $\delta r'$ due to guidance principle (method), the remainder is then the sum of the error due to the guidance system instruments. 25

For re-entry missiles, the normalized ballistic $\vec{r}_{\kappa}$ for the atmosphere re-entry stage may be established from $\vec{r}'$, $\vec{v}'$ determined from the externally measured data $\vec{r}$ from the real orbit. If an external ballistic tracking measurement is carried out on the position of the re-entry stage of the missile, then the deviation

$$\delta\vec{r}_{\kappa} = \vec{r}_{\kappa} - \vec{r}_{\kappa} \qquad (2\text{-}2)$$

is the so-called re-entry error due to the aerodynamic disturbance of re-entry. Or the re-entry error is the difference between the deviation of the impact point $\delta Q'$ calculated from $\delta i'$, $\delta r'$ and

the deviation δQ, of the actual point of impact.

We shall demonstrate the above principles with a re-entry missile as an example. Its orbit is shown in the above diagram.

III. DYNAMIC EQUATION FOR THE PROPULSION-FREE STAGE

We shall establish our dynamic equations in the vertical coordinate system Oxyz with the launching point 0 as the origin with oxz in the horizontal plane through 0 and ox basically along the flight direction. Oxyz rotates with the Earth. The propulsion-free stage (free flight stage) starts from the thrust ending at point K, through the ascending stage, the descending stage, at the re-entry stage and ends with the point 1 on Earth. The vehicle is acted on by gravitational force, centrifugal force, Copernican force and aerodynamic force. The propulsion-free dynamic equations are obtained after the aerodynamic lift force and side force:

initial condition $t^f = t_o^b$

$$\left.\begin{array}{ll}
\dot{x}=V_x & x' \\
\dot{y}=V_y & y' \\
\dot{z}=V_z & z' \\
\dot{V}_x=-\frac{1}{m_f}C_f\frac{\rho_0 S_f}{2}\cdot\left(\frac{\rho}{\rho_0}\right)\cdot V\cdot V_x-\dot{V}_{qx}-\dot{V}_{cx}+g_{xd} & V_x' \\
\dot{V}_y=-\frac{1}{m_f}C_f\cdot\frac{\rho_0 S_f}{2}\left(\frac{\rho}{\rho_0}\right)V\cdot V_y-\dot{V}_{qy}-\dot{V}_{cx}+g_{yd} & V_y' \\
\dot{V}_z=-\frac{1}{m_f}C_f\cdot\frac{\rho_0 S_f}{2}\left(\frac{\rho}{\rho_0}\right)V\cdot V_z-\dot{V}_{qz}-\dot{V}_{cz}+g_{zd} & V_z'
\end{array}\right\} \qquad (3\text{-}1)$$

where m_f, S_f, C_f are respectively the mass, reference cross-sectional area and aerodynamic frictional coefficient during the propulsion-free stage. x, y, z and V_x, V_y, V_z are the position and velocity components of the vehicle in Oxyz.

The linking acceleration components are:

$$\left.\begin{aligned}\dot{V}_{ex}&=\omega^2[b_x\zeta-(x+x_0)];\\ \dot{V}_{ey}&=\omega^2[b_y\zeta-(y+y_0)];\\ \dot{V}_{ez}&=\omega^2[b_z\zeta-(z+z_0)];\end{aligned}\right\} \tag{3-2}$$

where ω is the rotational angular velocity of Earth and the flight direction coefficients are

$$\left.\begin{aligned}b_x&=\cos W_t\cos A_m\\ b_y&=\sin W_t\\ b_z&=-\cos W_t\sin A_m\end{aligned}\right\} \tag{3-3}$$

W_t is the astronomical longitude of the point 0. A_m is the astronomical position angle of ox. The components of the radial distance EO of the point 0 to the center of the Earth in Oxyz are:

$$\left.\begin{aligned}x_0&=-R_{01}\sin\mu_0\cos A_m\\ y_0&=R_{01}\cos\mu_0\\ z_0&=R_{01}\sin\mu_0\sin A_m\end{aligned}\right\} \tag{3-4}$$

$$R_{01}=R_0+H_0$$

26

H_e is the height of point 0. The radial distance of any point on the Earth's ellipsoid of rotation is

$$R=\frac{R_e\sqrt{1-e^2}}{\sqrt{1-e^2\cos^2\phi_x}} \tag{3-5}$$

Earth center longitude:

$$\phi_x=\sin^{-1}\frac{\zeta}{r} \tag{3-6}$$

The equator surface height:

$$\zeta=b_x x+b_y y+b_z z+R_{01}\sin\phi_x \tag{3-7}$$

The radial distance of the vehicle position:

$$r=\sqrt{(x+x_0)^2+(y+y_0)^2+(z+z_0)^2} \tag{3-8}$$

The difference μ between the geographical longitude and the Earth center longitude of a point on Earth surface is calculated by:

$$\sin\mu=a_4\sin 2\phi_x=a_4\sin 2W_t \tag{3-9}$$

The geographical longitude at the launch point is taken as $W_n = W_t$. Equation (3-9) is used to compute μ_0,

$$\phi_{m_0} = W_t - \mu_0 \tag{3-10}$$

The relative velocity of the vehicle

$$V = \sqrt{V_x^2 + V_y^2 + V_z^2} \tag{3-11}$$

The coperican acceleration components are

$$\left.\begin{aligned} \dot{V}_{cx} &= 2\omega(b_2 V_z - b_3 V_y), \\ \dot{V}_{cy} &= 2\omega(b_3 V_x - b_1 V_z), \\ \dot{V}_{cz} &= 2\omega(b_1 V_y - b_2 V_x). \end{aligned}\right\} \tag{3-12}$$

The gravitational acceleration of an ellipsoid:

$$g_{\nu d} = g_e \frac{\nu_1}{r}\left[-\frac{R_e^2}{r^2} + J\frac{R_e}{r^4}\left(5\frac{\zeta^2}{r^2} - 1\right)\right], \tag{3-13}$$

$$(\nu = x,\ y,\ z;\ \nu_1 = \nu + \nu_0)$$

where R_c is the equatorial radius of Earth, $g_e R_e^2 = GM$ is the gravitational constant of Earth. a_d is the oblateness of Earth.

With the given initial conditions at $t = t' = t_0'$, the dynamic equations (3-1) are solved to obtain the diagram in the last section, called the normalized or reference orbit. From the normalized orbit, the velocity $\vec{V}(V_x, V_y, V_z)$ and position $\vec{r}(x, y, z)$. of the vehicle at any arbitrary time may be obtained.

IV. STATE TRANSFORMATION MATRIX

At $t' = t_0'$, the orbital parameter deviations are given. For example,

$$\begin{aligned} &\Delta V_x' = 10^{m/s}, \quad &&\Delta V_y' = 10^{m/s}, \quad &&\Delta V_z' = 10^{m/s}, \\ &\Delta x' = 1000^m \quad &&\Delta y' = 1000^m \quad &&\Delta z' = 1000^m; \end{aligned}$$

Taking one of these at a time, we can calculate 6 deviation orbits and also the state transformation matrix at each time instant on the orbit $B_i = (\cdot)_{6\times 6}$. For example, at the point 1 (i=1) at t = t_1: 27

$$B_1 = \begin{bmatrix} b_{11}' & b_{12}' & b_{13}' & b_{14}' & b_{15}' & b_{16}' \\ b_{21}' & b_{22}' & b_{23}' & b_{24}' & b_{25}' & b_{26}' \\ b_{31}' & b_{32}' & b_{33}' & b_{34}' & b_{35}' & b_{36}' \end{bmatrix} \tag{4-1}$$

At point (t = t_m), it is

$$B_m=\begin{bmatrix} b_{11}^m & b_{12}^m & b_{13}^m & b_{14}^m & b_{15}^m & b_{16}^m \\ b_{21}^m & b_{22}^m & b_{23}^m & b_{24}^m & b_{25}^m & b_{26}^m \\ b_{31}^m & b_{32}^m & b_{33}^m & b_{34}^m & b_{35}^m & b_{36}^m \end{bmatrix} \tag{4-2}$$

where

$$\begin{aligned} b_{ik}^l &= \frac{\partial x}{\partial \lambda^l} = \frac{x^l - \bar{x}^l}{\Delta \lambda^l} = \frac{\Delta x^l}{\Delta \lambda^l}, \\ b_{ik}^l &= \frac{\partial y}{\partial \lambda^l} = \frac{y^l - \bar{y}^l}{\Delta \lambda^l} = \frac{\Delta y^l}{\Delta \lambda^l}, \\ b_{ik}^l &= \frac{\partial z}{\partial \lambda^l} = \frac{z^l - \bar{z}^l}{\Delta \lambda^l} = \frac{\Delta z^l}{\Delta \lambda^l}; \end{aligned} \tag{4-3}$$

$$i=1,2,\cdots k\cdots l\cdots m\cdots n\cdots N,\quad k=1,2,3,4,5,6;$$

$$\lambda^l=(\lambda_k)_{6\times 1}=[\lambda_1\ \lambda_2\ \lambda_3\ \lambda_4\ \lambda_5\ \lambda_6]^T=[V_1^l\ V_2^l\ V_3^l\ x^l\ y^l\ z^l]^T,$$

$\bar{x}^l, x^l$ are the x values of point i at $t=t_1$ on the normalized orbit and the deviation orbit; correspondingly, $\bar{y}^l, y^l$ and $\bar{z}^l, z^l$ have the same meanings. Hence, the orbital parameter deviation vector or column matrix expressed with the transformation matrix is:

$$\Delta R^l = B_l \Delta \lambda^l \tag{4-4}$$

where

$$\Delta R^l=[\Delta r_1^l\ \Delta r_2^l\ \Delta r_3^l]^T=[\Delta x^l\ \Delta y^l\ \Delta z^l]^T, \tag{4-5}$$

For example, at point i = l

$$\Delta R^l=\begin{bmatrix} \Delta r_1^l \\ \Delta r_2^l \\ \Delta r_3^l \end{bmatrix}=\begin{bmatrix} \Delta x^l \\ \Delta y^l \\ \Delta z^l \end{bmatrix}=\begin{bmatrix} b_{11}^l & b_{12}^l & b_{13}^l & b_{14}^l & b_{15}^l & b_{16}^l \\ b_{21}^l & b_{22}^l & b_{23}^l & b_{24}^l & b_{25}^l & b_{26}^l \\ b_{31}^l & b_{32}^l & b_{33}^l & b_{34}^l & b_{35}^l & b_{36}^l \end{bmatrix}\begin{pmatrix} \Delta V_1^l \\ \Delta V_2^l \\ \Delta V_3^l \\ \Delta x^l \\ \Delta y^l \\ \Delta z^l \end{pmatrix} \tag{4-6}$$

The same form holds at i = m. We only need to change the superscript l into m. At points l and m, we have:

$$\Delta R^{lm}=\begin{pmatrix} \Delta r_1^l \\ \Delta r_2^l \\ \Delta r_3^l \\ \Delta r_1^m \\ \Delta r_2^m \\ \Delta r_3^m \end{pmatrix}=\begin{pmatrix} \Delta x^l \\ \Delta y^l \\ \Delta z^l \\ \Delta x^m \\ \Delta y^m \\ \Delta z^m \end{pmatrix}=\begin{pmatrix} b_{11}^l & b_{12}^l & b_{13}^l & b_{14}^l & b_{15}^l & b_{16}^l \\ b_{21}^l & b_{22}^l & b_{23}^l & b_{24}^l & b_{25}^l & b_{26}^l \\ b_{31}^l & b_{32}^l & b_{33}^l & b_{34}^l & b_{35}^l & b_{36}^l \\ b_{11}^m & b_{12}^m & b_{13}^m & b_{14}^m & b_{15}^m & b_{16}^m \\ b_{21}^m & b_{22}^m & b_{23}^m & b_{24}^m & b_{25}^m & b_{26}^m \\ b_{31}^m & b_{32}^m & b_{33}^m & b_{34}^m & b_{35}^m & b_{36}^m \end{pmatrix}\begin{pmatrix} \Delta V_1^l \\ \Delta V_2^l \\ \Delta V_3^l \\ \Delta x^l \\ \Delta y^l \\ \Delta z^l \end{pmatrix} \tag{4-7}$$

This may be expressed with sub-matrices as follows:

$$\Delta R^{1\sim m}=\begin{bmatrix}\Delta R^{1}\\ \Delta R^{m}\end{bmatrix} \tag{4-8}$$

$$B_{1\sim m}=\begin{bmatrix}B_1\\ B_m\end{bmatrix} \tag{4-9}$$

28

$\Delta R^{i}(i=1,m)$, as shown in (4-5). $B_i(i=1,m)$ as shown in (4-1) or (4-2). The sub-matrices B_1 and B_m are both 3x6 rectangular matrices. The sub-matrices ΔR^1 and ΔR^m are both 3x1 row matrices. Hence

$$\Delta R^{1\sim m}=B_{1\sim m}\Delta\lambda^{f} \tag{4-10}$$

where $\Delta\lambda^f$ is still a 6x1 row matrix.

$$\Delta\lambda^{f}=[\Delta\lambda_1,\Delta\lambda_2,\Delta\lambda_3,\Delta\lambda_4,\Delta\lambda_5,\Delta\lambda_6]^T=[\Delta V_x^f,\Delta V_y^f,\Delta V_z^f,\Delta x^f,\Delta y^f,\Delta z^f]^T \tag{4-11}$$

The super-script T outside the square bracket means the transpose of the matrix.

V. CALCULATION OF THE ORBITAL PARAMETER DEVIATIONS AT THE THRUST ENDING TIME t^f

The position vector components of the vehicle at $t = t_i$ during the propulsion-free stage are measured with radar or an optical system. The vector or matrix is

$$S^{i}=R_i^{i}+v^{i} \tag{5-1}$$

where

$$R_i^{i}=[x_i^{i},y_i^{i},z_i^{i}]^T \tag{5-2}$$

is the actual position of the vehicle at point i during the propulsion-free stage, v^i is the random measurement error of the measuring instrument

$$v^{i}=[v_x^{i},v_y^{i},v_z^{i}]^T \tag{5-3}$$

Generally, the average or mathematical expectation of the measurement error is assumed to be zero. The difference between the components of the actual orbit and the normalized orbit is

$$\left.\begin{aligned}\Delta x_i^{i}&=x_i^{i}-\tilde{x}^{i}\\ \Delta y_i^{i}&=y_i^{i}-\tilde{y}^{i}\\ \Delta z_i^{i}&=z_i^{i}-\tilde{z}^{i}\end{aligned}\right\} \tag{5-4}$$

simplified in matrix form as

$$\Delta R_i^{i}=[\Delta x_i^{i},\Delta y_i^{i},\Delta z_i^{i}]^T \tag{5-5}$$

similar to (4-6)

$$\Delta R^i = B_i \Delta\lambda^f \tag{5-6}$$

The deviation of the measured value S^i is

$$\Delta S^i = \Delta R^i + \nu^i = B_i \Delta\lambda^f + \nu^i \tag{5-7}$$

Now $\Delta\lambda^f$ is the unknown to be found. Expressed by $\Delta\lambda_1$, we get

$$B_i \Delta\lambda_1 = \Delta S^i - \nu^i \tag{5-8}$$

$$\Delta\lambda_1 = [\Delta V_{x_1}\ \Delta V_{y_1}\ \Delta V_{z_1}\ \Delta x_1\ \Delta y_1\ \Delta z_1]^T \tag{5-9}$$

If there is only one observation point 1, then

$$B_1 \Delta\lambda_1 = \Delta S^1 - \nu^1 \tag{5-10}$$

It is an equation system with 3 equations but 6 knowns. $\Delta\lambda_1$ is undetermined.

If there are 2 points of observation 1, m, i.e., observed values at two times t_1 and t_m, then

$$B_{1m} \Delta\lambda_1 = \Delta S^{1m} - \nu^{1m} = \Delta R^{1m} \tag{5-11}$$

Its equation number and unknown number are both 6. When the angle of the two points 1, m subtended at the center of the Earth is large enough, i.e., larger than 1 degree, the matrix B_{1m} is non-singular. Hence, the $\Delta\lambda_1$ to be found is definitely

$$\Delta\lambda_1 = (B_{1m})^{-1}(\Delta S^{1m} - \nu^{1m}) \tag{5-12}$$

It is the deviation of the orbit parameter that satisfies the guidance condition at the moment when the thrust ends and that we desire to calculate in the section "Discussion of the Basic Principles". Velocity deviation is

$$\Delta\bar{V}^i = V^i - \bar{V}^i = [\Delta V_x^i\ \Delta V_y^i\ \Delta V_z^i]^T = [\Delta V_{x_i}\ \Delta V_{y_i}\ \Delta V_{z_i}]^T \tag{5-13}$$

and position deviation is

$$\Delta\bar{r}^i = r^i - \bar{r}^i = [\Delta x^i\ \Delta y^i\ \Delta z^i]^T = [\Delta x_i\ \Delta y_i\ \Delta z_i]^T \tag{5-14}$$

When $\nu^1 \neq 0, \nu^m \neq 0$, the value found from (5-8) contains errors, and is not the true value of $\Delta\lambda^f$.

If the number of observation points N is larger than 2, then the data for any two distinct points 1, m may be used to calculate a set of $\Delta\lambda_1^i$ with (5-8). Then a better estimated value for $\Delta\lambda_1^f$ is

$$\Delta\bar{\lambda}_1 = \frac{1}{p}\sum_{i=1}^{p}\Delta\lambda_1^i \tag{5-15}$$

29

where p > 2 is the number of observation points.

If there is a large number of observation points S, i = 1, 2... k...l...m...n...N, then after numerical treatment, we can get the best estimated value of $\Delta\lambda^f$ to be $\Delta\lambda_2$. For each i point, equation (5-7) holds. The ΔS^i of N points has the same form

$$\Delta S = B\Delta\lambda_2 + \nu \tag{5-16}$$

where

$$\Delta S = [\Delta S^1\ \Delta S^2 \cdots \Delta S^k \cdots \Delta S^l \cdots \Delta S^m \cdots \Delta S^n \cdots \Delta S^N]^T \tag{5-17}$$

is a 3N x 1 row matrix. The submatrices ΔS^i are 3 x 1 row matrices. The transformation matrix B is formed from 3 x 6 rectangular matrices B_1.

$$B = [B_1 \cdots B_k \cdots B_l \cdots B_m \cdots B_n \cdots B_N]^T \tag{5-18}$$

Apparently, b is a 3N x 6 matrix. B are still computed from (4-1) or (4-2) and (4-3). $\Delta\lambda_2 = [\Delta V_{x_1}, \Delta V_{y_1}, \Delta V_{z_1}, \Delta x_2, \Delta y_2, \Delta z_2]^T$ is a 6 x 1 row matrix. When N > 2, equation (5-16) must be over-determined after expansion, i.e., the number of equations 3N is far greater than 6, the number of unknowns $\Delta\lambda_2$. The order of the matrix B = row number = 6. (The so-called order is the large order of the non-zero sub-matrix of B). According to matrix theory, it can be proved that

$$B^T B = F \tag{5-19}$$

is a non-singular symmetric matrix of order 6, i.e., the determinant

$$|F| = |B^T B| \neq 0 \tag{5-20}$$

Hence, the inverse matrix

$$F^{-1} = (B^T B)^{-1} \tag{5-21}$$

exists, and is the only matrix of order 6. Obviously, B^T is a 6 x 3N rectangular matrix. Multiplying equation (5-16) on the left by B^T, we have

$$B^T \Delta S = B^T B \Delta\lambda_2 + B^T \nu \tag{5-22}$$

After transposition, we get

$$B^T B \Delta\lambda_2 = B^T (\Delta S - \nu) \tag{5-23}$$

Multiplying (5-23) on the left by $(B^T B)^{-1}$, we have

$$\Delta\lambda_2 = (B^T B)^{-1} B^T (\Delta S - \nu) \tag{5-24}$$

This is the basic equation of the best estimated value when we calculate $\Delta\lambda^f$ with a large amount of data. Statisticians call (5-24) the normalized or normal equation, and also the wave filter equation. It will reduce the effect of the random error ν on $\Delta\lambda_2$. If the square difference of each observation point i of the measurement system is known, better results will be obtained by weighting each point in (5-24) according to the square difference.

After expansion, it may be shown that (5-24) may be expressed as the sum of the corresponding form s of the sub-matrices at a point i:

$$\Delta\lambda_2=(B^TB)^{-1}(B^T[\Delta S-\nu])=\left(\sum_{i=1}^{N}B_i^TB_i\right)^{-1}\left(\sum_{i=1}^{N}B_i^T[\Delta S_i-\nu_i]\right) \tag{5-25}$$

Results similar to equation (5-24) and (5-25) may be obtained by using the least square method in detailed derivations.

VI. TOTAL SYSTEM ERROR

If the time that the command for shutting off the engine by the guidance system, t_k is before the time t^f when the vehicle thrust ends, then it is necessary to delete the effect $\Delta\lambda_k$ of the thrust in the interval (t_k,t^f) (i.e., the usually mentioned after-effect thrust) on the orbital parameters from $\Delta\lambda^f$ by using the remotely measured or externally measured parameters so that we may obtain the orbital parameter deviation caused by the total system error:

$$\Delta\lambda^A=\Delta\lambda^f-\Delta\lambda_k \tag{6-1}$$

$\Delta\lambda^f$ is replaced by the $\Delta\lambda_2$ calculated with (5-25). The total guidance error or synthetic guidance error is

$$\Delta Q=\sum_{i=1}^{n}\frac{\partial Q}{\partial\lambda_i}\Delta\lambda_i \tag{6-2}$$

ΔQ denotes the circular error or the deviation of the transverse and longitudinal impact points. The partial derivative is found from the calculation of deviation orbit.

VII. CONCLUSIONS

The main ideas of the "basic principles", equations (4-6), (6-1 and (6-2) and the measurement requirements in this paper had been published in 1975. In recent years, large volumes of experiments, the measurement of orbital parameters during propulsion-free stage and calculation of the impact point deviation indicate that the above theory is correct, and may be used as an auxiliary method to judge the accuracy of the guidance system.

From the diagram, it can be obviously seen that the data for the descending stage will yield better analytical results than those for the ascending stage.

The proposal, organization, implementation and perfection of this method is the joint effort of many comrades, including Wang Meizhi, Wu Jiren, Zhou Taiping, etc. The author only made some derivations and explanations.

REFERENCES

A.A. Dimitrilievskiy, External Ballistic, Defense Industry Publisher

B. Wavlomiyenyev Ballistic Missile Design and Testing, Defense Industry Publisher

C. A. Gaurbachinko et al. Handbook of Flight Dynamics (I) Defense Industry Publisher

Xie Bangjie . Linear Algebra, People's Education Publisher

Lectures on Ground Measurements, edited by Wuhan College of Survey, Surveying Publishing House.

COMPUTER SIMULATION OF LIQUID ROCKET ENGINE TRANSIENTS

Wang Kechang 3769 0344 2460
(xx xx, xxxx)

Abstract

In this paper the transients are simulated by means of the characteristic method and the numerical computation method for start and shutdown processes, pulse operation, four-engine parallel operation and failure state of liquid rocket engine. Simulation is made on the computer "441B-III". The simulated results show that in the engine development computer simulation would be necessary.

TABLE OF SYMBOLS

A channel cross-sectional area
a sound velocity of propellant in the channel
c_1, c_2, c_3 coefficients
D channel diameter
E elastic modulus
f frictional coefficient of flow
g gravitational acceleration
K fluid bulk modulus
Q volume flow rate
P pressure
t time
e channel wall thickness density
r specific gravity
θ channel inclination angle
ρ density

I. INTRODUCTION

The operational status of liquid propellant rocket engines of various types consists of pulsed operation, multiple start, multiple engine parallel operation, variable propulsion operation, etc. For various types of engines, it is required that they have good dynamic properties during start, shut down and propulsion adjustment, which is to say that they should have satisfactory transient operational processes. Hence, the transient processes of a liquid propellant rocket engine represent a very important aspect of rocket

engine research. Many people have long been searching for the laws of nature in this area. However, because the study of these transient processes involves the dynamic equations of the various parts of the engine, where the channel equation of the supply system is a system of hyperbolic partial differential equations, it was very difficult to carry out such kinds of computational research work before the wide spread use of the electronic computers. It was in the 60's, following the appearance of the electronic computers, that ground was broken in implementing the kind of calculations mentioned above. Many papers describing computational study in this area appeared between 1968-1970 with satisfactory results.

R. J. Dorsch and D. J. Wood [1] used the wave-plane method to analyze the nonstationary channel flow and computed the parameters of the propellant supply system of the liquid propellant rocket engine.

John J. Boehnlein [2] et al used the Laplace transform to solve the channel wave equation, analyzed the nonstationary flow in the channel and computed the starting transient process of the liquid propellant rocket engine with satisfactory result.

J. C. Eschweiler, H. W. Wallace [3], P. F. Thompson, T. J. Walsh [4] used the characteristics linear method to solve the channel nonstationary flow, and simulated the transient operational process of the liquid propellant rocket engine on the computer with good results.

In these papers, simple mathematical models are used to treat the combustion chamber dynamic equation. But W. T. Webber, W. A. Gaubatz [5] did a lot of work on the model of the combustion chamber while comrades Yang Benlian and Chen Guotai did a large amount of valuable computational work [6] with reference [5] as the foundation. In this paper, we also start with the characteristics line method with a list of the various commonly used boundary conditions in

*Received August 29, 1980

liquid propellant rocket engines, and simulated on the 441b-I computer the transient processes of start, shut down, pulsed operation, multiple engine parallel operation and engine fault state, resulting in a list of simulation curves for the various situations.

II. BASIC EQUATIONS

The basic equations used in analyzing the engine transient processes are mainly the differential equations for the nonstationary fluid flow. [7] has given a detailed derivation. Here we shall just list

$$\frac{Q}{A}\frac{\partial Q}{\partial X}+\frac{\partial Q}{\partial t}+\frac{A}{\rho}\frac{\partial P}{\partial X}+\frac{f}{2DA}Q|Q|-Ag\sin\theta=0 \tag{2-1}$$

the continuity equation:

$$\frac{1}{\rho}\left(\frac{Q}{A}\frac{\partial P}{\partial X}+\frac{\partial P}{\partial t}\right)+\frac{a^2}{A}\frac{\partial Q}{\partial X}=0 \tag{2-2}$$

This is a set of hyperbolic partial differential equations for which it is generally rather difficult to find accurate closed solutions. [7] gave a detailed description of solving these equations with the characteristics method. We shall only list the final results:

$$\left.\begin{aligned} &P_P-P_A+\frac{\rho a}{A}(Q_P-Q_A)+\frac{f\rho a}{2DA^2}Q_A|Q_A|\,\Delta t=0\\ &\Delta X=a\Delta t\end{aligned}\right\}C^+ \tag{2-3}$$

$$\left.\begin{aligned} &P_P-P_B-\frac{\rho a}{A}(Q_P-Q_B)-\frac{f\rho a}{2DA^2}Q_B|Q_B|\,\Delta t=0\\ &\Delta X=-a\Delta t\end{aligned}\right\}C^- \tag{2-4}$$

where P_A, P_B, P_p represent respectively the pressure at points A, B and P.

Q_A, Q_B, Q_p represent respectively the bulk flow rate of the points A, B and P in Figure 1. (P_A, P_B, Q_A, Q_B are known. They may be determined from the initial conditions or calculated from the previous time interval).

It should be noticed that the first equation in Equation (2-3) is only true along the +ve characteristic line AP. Similarly, the first equation of equation (2-4) is only true along the -ve characteristics BP. As there are only two unknowns Q_p,P_p in equation (2-3) and equation (2-4), therefore Q_p and P_p may be found from equation (2-3) and equation (2-4). In order to facilitate the writing of the computer programs, we give below a computational equation for expressing the parameters of the ith section channel flow. Substituting the symbols, as shown in Figure 2 into the first equations of equations (2-3) and (2-4), we get

33

$$Q_{Pi}=0.5\left[Q_{i-1}+Q_{i+1}+\frac{A}{a\rho}(P_{i-1}-P_{i+1})\right.$$
$$\left.-\frac{f\Delta t}{2DA}(Q_{i-1}|Q_{i-1}|+Q_{i+1}|Q_{i+1}|)\right] \qquad (2\text{-}5)$$

$$P_{Pi}=0.5\left[P_{i-1}+P_{i+1}+\frac{a\rho}{A}(Q_{i-1}-Q_{i+1})\right. \qquad (2\text{-}6)$$
$$\left.-\frac{af\rho\Delta t}{2DA^2}(Q_{i-1}|Q_{i-1}|-Q_{i+1}|Q_{i+1}|)\right]$$

where

Q_{Pi}, P_{Pi} —— are the flow parameters of the ith channel section at the time instant to be computed

Q_{i-1}, P_{i-1} —— are the flow parameters of the i-1th channel section at the time instant previous to that being computed

(2-5),(2-6) are the folow parameters pf the i+1th channel section at the time instant previous to that being computed.

Equations (2-5), (2-6) are the computational equations that we will use frequently from now on to compute the mid-point flow parameters.

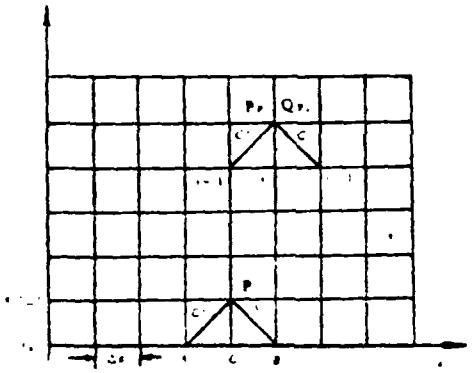

Figure 1. Characteristic grid

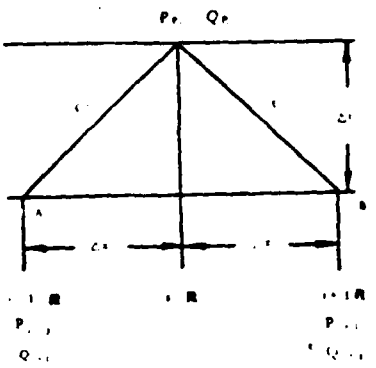

Figure 2. Grid for finding the mid-point

III. BOUNDARY CONDITIONS

Equations (2-5), (2-6) can only be used to calculate the flow parameters at the mid-point of each computed channel. But we shall discover that at either end of the computed channel there is only one characteristics equation (C^+ or C^-) that can be used. The C^- characteristics equation can only be used upstream while the C^+ characteristics equation can only be used downstream. However, with one equation it is impossible to find two unknowns (Q_p,P_p). Thus, it is necessary to establish an equation to connect the two unknowns. The boundary condition problem is, therefore, involved. The setup of the boundary conditions and flow system is closely related to the forms of the object. Detailed descriptions of various boundary conditions for the general hydroelectric power systems have been presented in [8] and [9]. But as shown in Figure 3, the liquid propellant rocket engine system is a complicated system with boundary conditions of diverse types.

References [7,11,12] have derived in detail the various boundary conditions of liquid propellant rocket engine systems. These boundary conditions involve the following principal objects. They are: the propellant storage tank, the valve or flow regulating orifices in the channel, the sprayer, the propellant liquid collection chamber, channel connectors (3 channel, 5-channel, etc.), cooling

jacket, energy storage unit, centrifuge, etc. We shall only point out a few important points here:

1. All boundary conditions are treated similarly. They are mainly applied to the C^+ or C^- characteristics equations. Then the equation connecting Q_p,P_p, (such as the sprayer equation, the valve equation or the centrifuge equation, etc.) is listed based on the shape of the object at the boundary. The equations are then solved simultaneously by using the continuity relations to obtain the pressure (P_p) and flow rate (Q_p) at the boundary.

2. The equation thus solved is usually a quadratic equation with one unknown. The solution can be easily found. Only the boundary condition of the energy storage unit gives a nonlinear equation which we solved with the Newton approximation method.

3. The boundary condition equations listed in [7,11,12] have been used in extensive computations on the computer. The results show that these equations can be used.

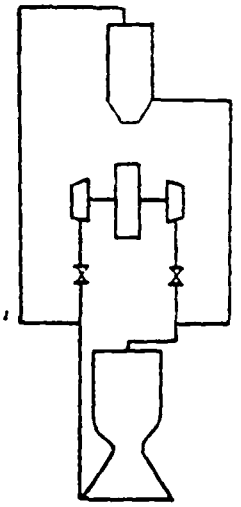

Figure 3. Simplified diagram of the supply system of two elements liquid fuel rocket engine.

IV. COMPUTER SIMULATION OF VARIOUS TRANSIENTS OF A LIQUID PROPELLANT ROCKET ENGINE

1. Determination of time increment Δt and number of section N.

The supply system of the liquid propellant rocket engine is a complicated system, composed of many channels and the lengths of each channel may differ greatly. Before proceeding with the simulation, the problem of determining and selecting the time increment Δt and how to divide the channels into sections is encountered.

Firstly, the time increment for each channel should be the same so that the boundary conditions can be used. At the same time, the Courant stability condition [9] must be satisfied in selecting the time increment, namely:

$$\frac{\Delta t}{\Delta x} \leq \frac{1}{a} \tag{4-1}$$

This indicates that Δx must be greater than or equal to $a.\Delta t$. Hence, the selection of Δt under the condition that the speed of sound is already determined is mainly limited by Δx while Δx must be constrained by the shortest channel in the system. If the shortest channel is short, then Δx will be small and Δt cannot be taken very large. When Δt is small, the computational time and expense will increase so that for a large number of channels, the fine division may even exceed the memory of the computer. Based on our experience, we think that Δt should be chosen as follows. Firstly, the system channels should be analyzed to find the shortest one. If this channel is indeed too short, then it should be treated separately by the finite difference method similarly to the procedure for the sprayer liquid collector chamber. If this short channel is not too short, then it may be treated in two sections, from which a Δt value will be found.

$$\Delta t = \Delta x \cdot \frac{1}{a} \tag{4-2}$$

This Δt then can be used for the whole system.
However, we must notice that:

1) After Δt is determined by analyzing the shortest channel, in general, it will not change any more. Then the other channels may be treated by the following method:

35

$$N_i = \frac{L_i}{a_i \Delta t} \tag{4-3}$$

N is the number of divisions of the ith channel and should be an integer. But the N value found from equation (4-3) is often non-integer. Hence, both V. L. Streerer and M. H. Chaudry have pointed out that due to the approximate nature in the calculation of a, i.e.,

its value cannot be accurately known, therefore, it is possible to adjust the value of speed of sound approximately to make N value an integer.

2) We have carried out comparison computations on the computer on the effect of the number of divisions of the shortest channel and discovered that when N was taken to be 2 and 10 the results were very close, which indicates that very accurate results are attainable when the number of divisions is reduced. Table 1 lists the data of the analytical calculations of engine disturbance for comparison.

TABLE 1. Comparison of the calculated values of the principal parameters ($\bar{P}_c$, $\bar{P}_r$, $\bar{n}$) for difference N

	10 ms			20 ms		
	$\bar{P}_c$	$\bar{P}_r$	$\bar{n}$	$\bar{P}_c$	$\bar{P}_r$	$\bar{n}$
$N=10$	0.9816	1.0024	0.9995	0.971	0.9994	0.999
$N=2$	0.9811	1.0018	0.9995	0.971	0.999	1.001

During the calculation, we found that the effect of decreasing the number of divisions is very attractive as long as satisfactory accuracy can be maintained. When N = 10, the time increment of the disturbance computations is Δt = 0.2 ms. To compute one Δt, it would take 55 seconds of computational time on the 441B-I computer, while for N = 2, the time increment Δt = 0.5 second and it only took about 10 seconds to compute one Δt. The total computational time for one engine disturbance was also reduced from three hours to half an hour. Thus, the choice of N (hence the determination of Δt) is a very important question, worthy of our attention.

2. Simulation of liquid propellant rocket engine start and shut-down.

Start and shut-down are two important transient processes of a liquid propellant rocket engine. They are related to the reliability of start, reliability of stage separation, etc. We have carried out calculations on the 441B-I computer of various types of start and shut-

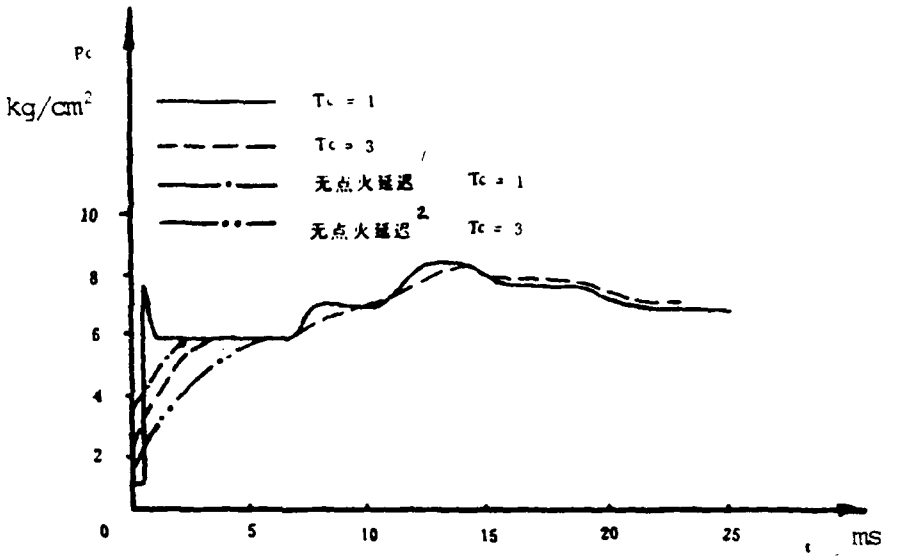

Figure 4. Curve of combustion chamber pressure (P_c) with time with the valve right next to the injector and no liquid collecting chamber
1--no ignition delay; 2--no ignition delay

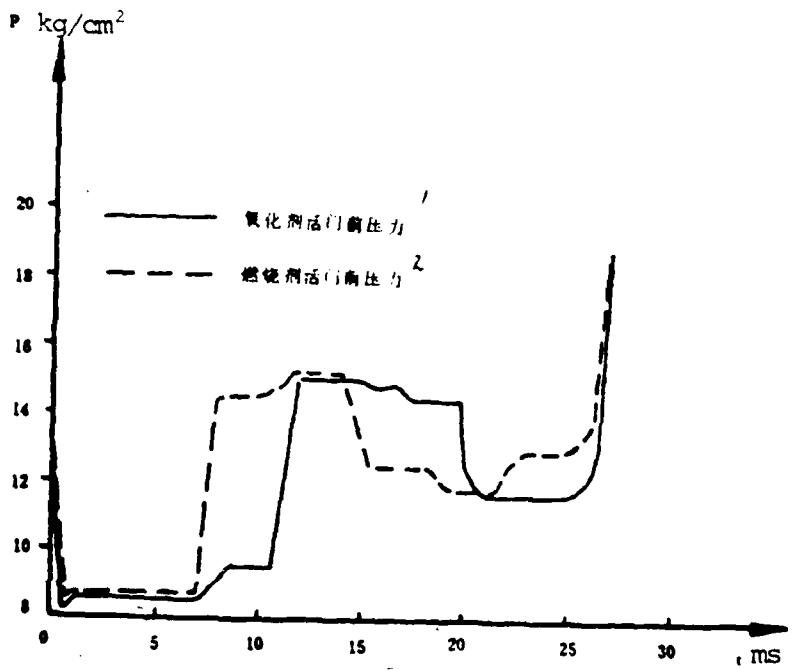

Figure 5. Curve of the pressure in front of the propellant valves versus time
1--pressure in front of the oxidizer valve;
2--pressure in front of the combustible valve

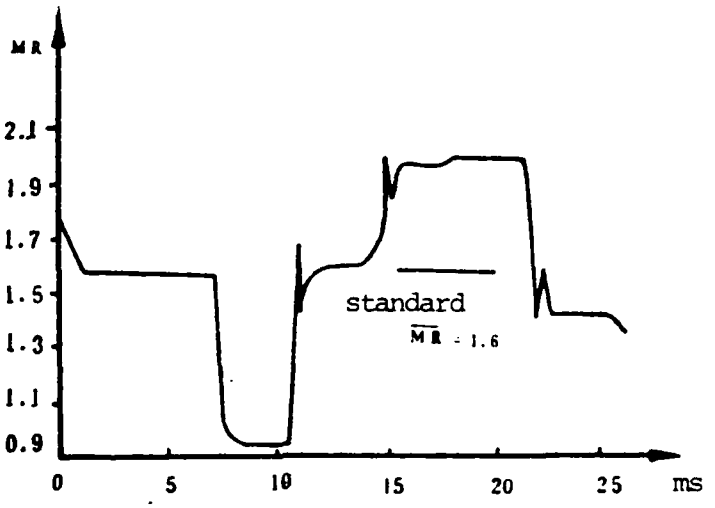

36

Figure 6. Curve of propellant component ratio with time

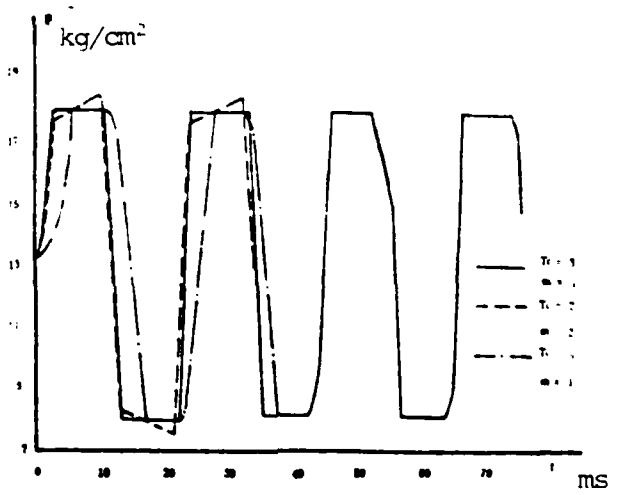

Figure 7. Curves of water impingement pressure in front of oxidizer valve after shut-down versus time.

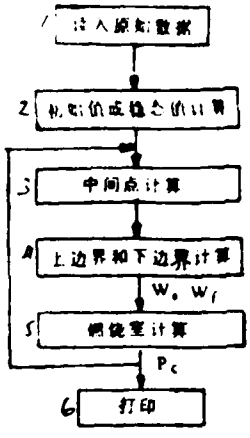

Figure 8. Overall flow chart of start computation
1--read in original data;
2--initial or stationary value calculation;
3--middle point calculation;
4--upper and lower boundary calculation;
5--combustion chamber calculation;
6--print out

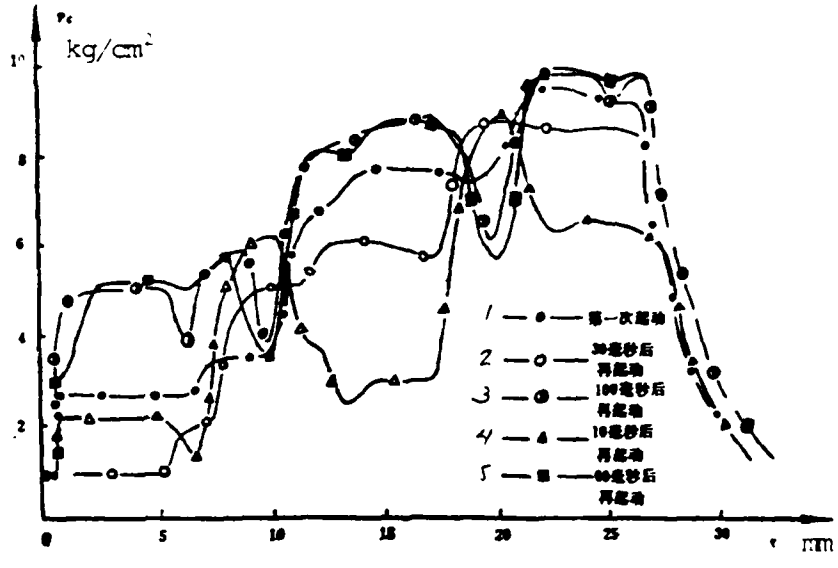

Figure 9. P_c-t curves for restart at different times
1--first start; 2--restart after 30 ms; 3--restart after 100 ms;
4--restart after 10 ms; 5--restart after 50 ms

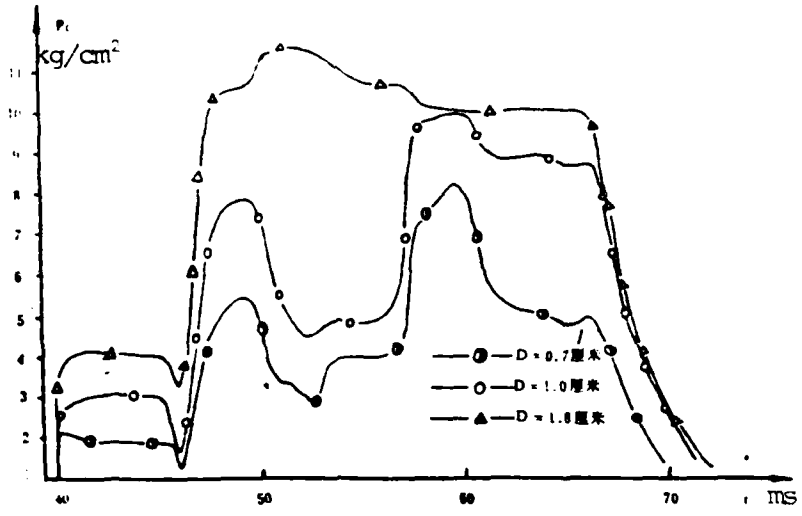

Figure 10. P_c-t curve for restart with different diameters at t=40 ms
1--cm

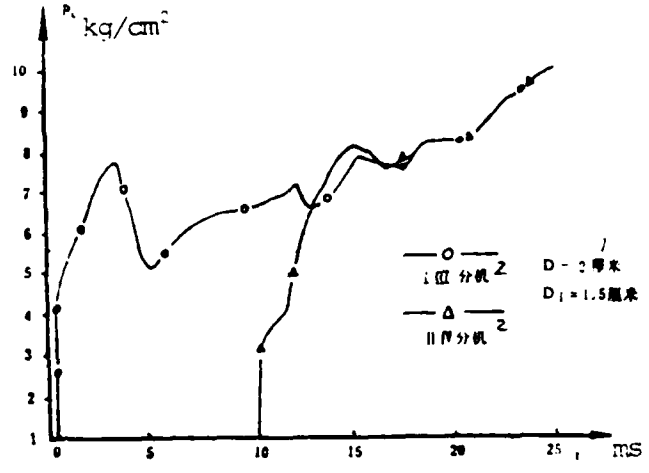

Figure 11. P_c-t curves for 4 engine parallel operation, restarting in two groups.
1--cm ; 2--engines

down processes for an attitude control engine with 11.35 kg of thrust, using N_2O_4 + R-NH-NH-50 as propellant. The results of the computation are shown as the curves in the following diagrams. Analysis on the result may be found in [7].

3. Simulation of the attitude control engine pulsed operation and 4 engine parallel operation transients.

The attitude control engine used on flying vehicles has the following characteristics. Firstly, the number of attitude control engines is large, usually 4 or more, and they all use the same propellant supply channel. As the attitude control engines do not usually start or shut-down at the same time, therefore, one must clearly understand the effect of start or shut-down of one or two engines on the operation of the other engines. The other characteristics of attitude control engines is the large number of re-starts. For instance, the number of starts of the attitude control engines on the Apollo may reach 100,000 and the operation frequency 40 times/sec. What is the effect of adjacent pulse operations on one another under this kind of operation frequency? In order to understand this problem, we separately simulated the following cases:

1) Restart 10 ms after the end of the first pulse. Here the pressure in the oxidizer is in the low pressure wave region and that in the combustible channel is in the high pressure wave region.

2) Restart 30 ms after the end of the first pulse. Here the pressures in both the oxidizer and combustible channels are in the low pressure wave region.

3) Restart 60 ms after the end of the first pulse. Here the pressure in the oxidizer channel is in the high pressure wave region and that in the combustible channel is in the low pressure wave region.

4) Restart 100 ms after the end of the first pulse. Here the pressures in both the oxidizer and combustible channels are in the high pressure wave region.

5) Effect of channels of different diameters on the start process.

6) Two engines start first and after several ms, the other two engines will then start.

The results of the simulation are shown in the following curves. Analysis of the results may be found in [11].

4. Simulation of liquid propellant rocket engine fault state transient.

Analysis of liquid propellant rocket engine fault state is very important and very complicated. Fault analysis is involved from the beginning to the end in the test analysis of the engine on test stand and in the flight test analysis of the engine. In the test stand testing stage, it is still possible to use the high speed photography, experimental parameter curves recorded during the test and the engine itself after the test for a synthetic analysis. In the flight test, because it is difficult to find complete remains of the engine, we can only make our analysis based on the remote measurement data. Hence, if one can simulate with computation the transient processes of various important parameters of the engine (e.g., combustion chamber pressure, propellant flow rate, turbine rotational speed, etc.) under various fault conditions (e.g., channel leak, injector blockage, etc.), the analysis and research on engine fault will be greatly benefited since we only need to compare the transient curves of various parameters actually recorded during engine fault to those obtained from computational methods under various assumed fault conditions in order to determine the type and location of the fault. This will help in narrowing down the scope of analysis and reducing the work load for analysis, and hence will promote greatly the progress of engine development.

The computation of engine fault transients is primarily dependent upon the establishment of fault state computational model. In [12], an engine fault computational model of a medium thrust, pumped propellant with 2 engine group elements is presented. The following diagrams show the computational results. An analysis of the results may be found in [12].

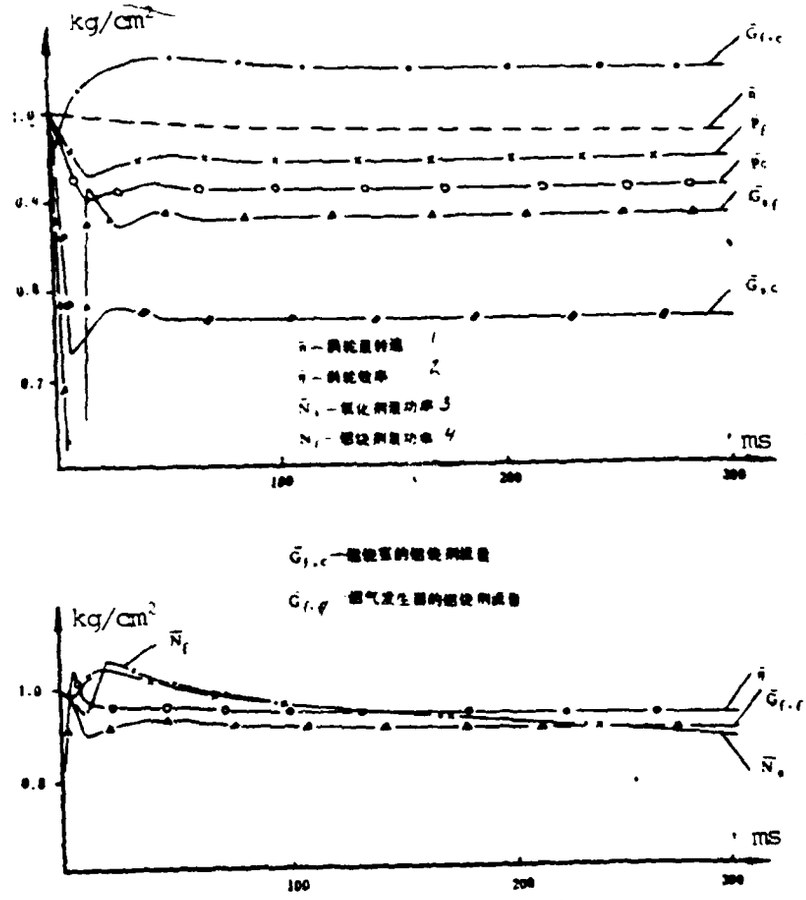

Figure 12. Transient during oxidizer channel leakage
1--pump rotational speed; 2--turbine efficiency; 3--oxidizer pump power; 4--fuel pump power; 5--combustion chamber fuel flow rate; 6--fuel flow rate in fuel vaporizer

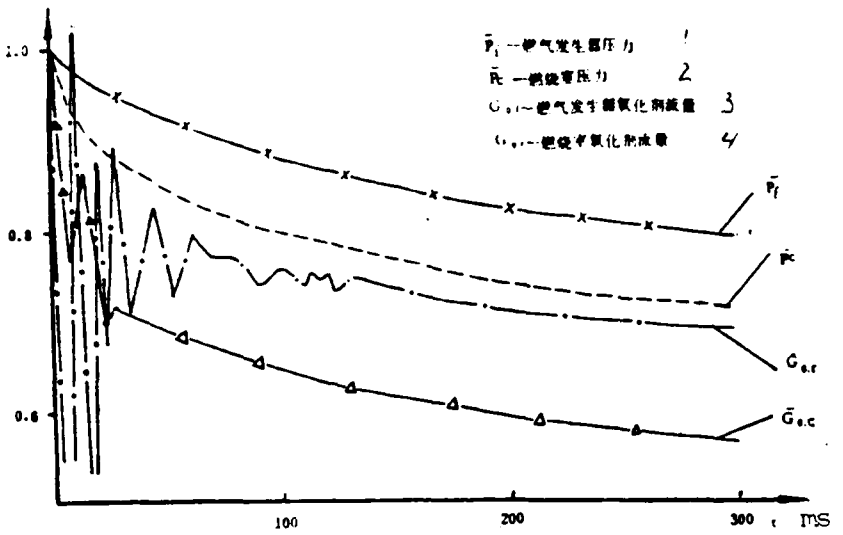

Figure 13. Parameter variation during oxidizer valve 1--fuel vaporizer pressure; 2--combustion chamber pressure; 3--oxidizer flow rate in fuel vaporizer; 4--combustion chamber oxidizer

V. CONCLUSIONS AND PROPOSALS

1. Computer modeling of liquid propellant rocket engines is very instructive in the development of the engine. It helps us in selecting the principal parameters, in proving the major plans and in predicting the whole transient process. Today when the application of the electronic computer is ever widening, computer modeling will become an important link in the design, development and experimentation of liquid propellant rocket engines.

2. The keys to the computer modeling of engine transients are (1) the establishment and gradual perfection of the mathematical model of various parts of the engine. For instance, there are now more than a dozen computational models for the combustion chamber computational model internationally. We should study and analyze these models to establish a mathematical model that fits our needs. (2) Development of the commonly used computer programs (including the study of the computational methods). (3) Supply of experimental

data for the various parts. For instance, it is still difficult to find the flow coefficient-time curve and the degree of openness vs. time curve during valve opening and closing. Much work needs to be done before computer modeling of engine transients can be perfected and used in practice. In this paper, we have only provided a rough outline. We welcome your criticism so that the work of computer modeling may be further developed.

REFERENCES

[1] R.G. Dorsch, D.J. Wood, Distributed Parameter Analysis of Pressure and Fow Disturbances in Rocket propellant feed systems, NASA TN D-3529, 1966.

[2] John J. Boehnlein, et al, Generlized Propulsion System Model for NASA Manned Spacecraft Center, NASA-CR-114915, 1971.

[3] J.C. Eschweiler, H.W. Wallace, "Liquid Rocket Engine feed System Dynamics by the Method ofCharacteristics," Transactions of the ASNE Series B Vol. 90. NO 4. 1968.

[4] P.F. Thompson, T.J. Walsh, Characterization of Attitude Control Propulsion Systems, NASA-CR-115183, 1971.

[5] W.T. Webber, W.A. Gaubatz, "Calculation of the Ignition and Start Transient of Liquid Propellant Rocket Engines," WSS/ci paper 70-23.

[6] Xiang Ben-lian, Chen Guo-tai, Computer Calculation of Hot Start and Shut Down of Liquid Fuel Rocket Engine, Journal of Engineering, 1979, 4

[7] Wang Ke-chang, Computation of the Start-up and Shut-down of Liquid Fuel Rocket Engine, Journal of Engineering, 1979, 4

[8] E.B. Wylie, V.L. Streeter, *Fluid Transients*, 1978.

[9] M.H. Chaudhry, *Applied Hydraulic Transients*. 1979.

[10] D.J. Wood, S.E. Jone, "Water Tammer Charts for Various Type of valve," ASCE Vol. 99 HY.1. pp 167178, 1973.

[11] Wang Ke-chang, Some Applications of Numerical Methods in Calculating the Transients of Liquid Fuel Rocket Engines, Journal of Engineering, 1979, 4

[12] Wang Ke-chang, Computer Model Analysis of the Fault State of Pump-Pressured Liquid Fuel Rocket Engine

REPEATED TRIAL OF GUIDANCE IN SPACE VEHICLES

He Lucheng

ABSTRACT

This article covers the advantages of the repeated method and the applications of the repeated method in strap-down inertial system. The differences of this method with those described in the previous article [1], [2] are:

1. Not only the reliability of the system, but also the accuracy of the system will be improved.

2. The key components which affect the accuracy in guidance should be repeatedly fit in the optimum directions and those which affect reliability should be considered to be in the orthogonal or non-orthogonal repeated method.

3. This article provides the method of inspecting failure by means of range and derives the formulae of calculating accuracy and effectiveness. This method will make calculation simple and work of the system reliable.

4. Applying the theory mentioned above, the error in guidance will be decreased by $\frac{1}{\sqrt{2}}$ and the ineffectiveness can also be decreased by two orders of magnitude, if a longitudinal accelerator and a two-freedom gyro are added to the strap-down guidance device.

I. Formulation of the problem

33

Repeated trial methods may be used to enhance the accuracy of space vehicle guidance by compensating for systematic errors and

*Received 15 June 1979

reducing random errors. The repeated trial method is not simply to enhance the accuracy by the $\sigma/\sqrt{n}$ method. It also compensates for the unknown systematic errors (gyro acceleration meters are installed with one normal and the other reversed and backward, so that when the data from the two meters are averaged, systematic errors are compensated) and cancels rolling error. The more important advantage of the repeated trial method is to improve reliability, as unreliability is potentially more harmful. The strap-down method eliminates the constant level platform and its stabilizing system. As electronic computers are being perfected and miniaturized, the weight and size of the strap-down inertial system may be made very small. The most important advantage of the strap-down inertial system is the ease in using the repeated trial method which greatly improves reliability.

II. Several repeated trials method

1. Arithmetic average method

In order to understand the advantages and disadvantages of various repeated trial methods, we shall first describe the error probability model of a single inertial assembly. For example, the error model of a gyro is

$$S = \sum_{i=1}^{K} (\omega_{i1} + \omega_{i2}) W_i = \bar{\omega}_1 \cdot \vec{W} + \tilde{\omega}_1 \vec{W} \qquad (1)$$

where "." means vector dot product, i.e., $X \cdot Y = \sum_{i=1}^{K} x_i \cdot y_i$ 34

$\vec{W}_i$ is the environmental factor, including the overload acceleration experienced by the sensor, as well as the coupling of accelerations along other directions, and such environmental stresses as temperature rise, vibrations and gas pressure.

$\bar{\omega}_1, \tilde{\omega}_1$ are the uncorrected error coefficient values corresponding to the environmental stress. $\bar{\omega}_1$ is the mathematical expectation, referred to below as regular error; $\tilde{\omega}_1$ is the random part. S_1 is the system output error.

Under the action of some environmental stresses, it is necessary to take the absolute value of some errors which can be transformed into regular errors and random errors. If the errors are independent and are composed of many small disturbances, then the error model may be written as

$$m = E[S] = \bar{\omega}_i \cdot \bar{W} \qquad (2)$$

$$\sigma = \sqrt{\sum_{i=1}^{\kappa} (\omega_{ii} \cdot W_i)^2} \qquad (3)$$

According to the Central Limit Theorem, normal distribution N(m, σ) must be satisfied. Many trials are performed on the same element under the influence of each environmental stress on the ground. Each environmental stress is

$$m_i = r_i \sigma_i \qquad (4)$$

m_i sometimes may be several times that of σ_i.

We try to find m to make corrections by using as much as possible the data of many trials and from ground signals, but sometimes it is not easy. However, if we use an even number of basically identical elements, with half of them normal and the other half reversed and backward, and then average the measured data, then the regular errors will be mostly cancelled and random error reduced. If the number of repetitions is n, then the random error will be reduced to $\frac{1}{\sqrt{n}}$. When this simple arithmetic averaging method is used on a certain object without too many measurements, any anomalous data can generally be detected by inspection. But for unmanned automatic guidance systems, any faulty data or data with large deviations must be instantly detected. The normal data are then averaged so that the accuracy and reliability of the system may be guaranteed. Otherwise, the average will be in error even if there should only be one piece of data with fault or with large deviations and the whole system may become ineffective. In this way, the ineffectiveness may be increased n times. The improvement of accuracy actually means the improvement of the probability of a successful mission, but arithmetic averaging may increase ineffectiveness. Sometimes the loss may be more than the gain.

In order to overcome the shortcomings of the arithmetic averaging method, the 0-1 checking method is proposed, in which data with large deviations are automatically detected and isolated. The basic logic is to permutate the data according to software programs and to subtract in pairs. When the difference exceeds a certain value, 1 is assigned; otherwise 0 is assigned. Then the location of an error is found based on the way 1's appear and is discarded.

In the strap-down guidance system, an orthogonal coordinate system is fixed on the vehicle. Each axis must complete automatic fault checking with respect to three fixed acceleration meters and three single-freedom gyros. In this way, the number of elements is increased three-fold. To reduce the number of elements, a regular dodecahedron scheme was proposed in reference [1] and a non-orthogonal system was proposed in reference [2]. Both of these will reduce the number of elements from three times to two times or less.

2. *Dodecahedron method*

Let Oxyz be a coordinate system fixed to the vehicle. The meter input axis is fixed to six axes $u_1, u_2, \cdots\cdots u_6$. u_1 and u_2 are in the xy plane making angles +a and -a with the x-axis. u_3, u_4, u_5, u_6 are similar as shown in the diagram.

Let $c = \cos a, s = \sin a,$. Then the visual acceleration a_x, a_y, a_z of the vehicle may be analyzed as

$$\begin{cases} u_1 = ca_x - sa_y + b_1 \\ u_2 = ca_x + sa_y + b_2 \\ u_3 = ca_y - sa_z + b_3 \end{cases}$$

$$\begin{cases} u_4 = ca_y + sa_z + b_4 \\ u_5 = ca_z - sa_x + b_5 \\ u_6 = ca_z + sa_x + b_6 \end{cases} \qquad (5)$$

35

or in matrix notation $\bar{u}=A\bar{x}+\bar{b}$

where $\bar{b}$ is the error matrix, $\bar{u}$ is the measurement matrix, A is the transformation matrix, $\bar{x}$ is the ballistic motion state. If the $\bar{u}$ data of the various meters are all normal, then by the least square method

$$\bar{x}=(A^TA)^{-1}A^T\bar{u} \qquad (6)$$

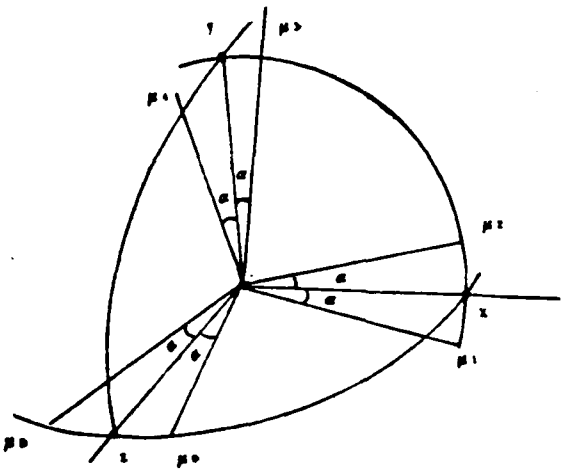

Theoretically, to solve three unknowns with six equations, a_x, a_y, a_z, a fault may be permitted to occur for three measured data. Reference [1] listed the fault data detection method. For example, from the u_1 and u_2 data in equation (5), we can estimate $\hat{a}_x=\frac{u_1+u_2}{2\cos\alpha}$, and from u_5 and u_6 in equation $\hat{a}_x=$ we can estimate $-\frac{u_5-u_6}{2A\sin\alpha}$.

If the difference between the 2 $\hat{a}_x$ exceeds the allowed range, then one or more of u_1, u_2, u_5 and u_6 are faulty. The same holds for the other u's. Finally, the fault location may be determined. If no more than three pieces of data are faulty in equation (5), then the computer program will check out the faulty equaton and discard it. Then the least square method is used again to solve for a_x, a_y, a_z.

3. Non-orthogonal system method [2]

An oblique set of axes is selected with unit vectors e_1°, e_2°, e_3° which satisfy

$$\begin{cases} e_i^\circ \cdot e_j^\circ \neq 0, \\ e_i^\circ \cdot e_i^\circ \neq 1, \end{cases} \qquad \text{when } i \neq j$$

i.e., the three axes are neither colinear nor mutually perpendicular. This is called a non-orthogonal system.

A unique reciprocal system $c_1^\circ, c_2^\circ, c_3^\circ$, may be determined for this non-orthogonal system satisfying the following relations:

$$e_i^\circ \cdot c_j^\circ = \begin{cases} \cos a_i, & \text{when } i = j \\ 0 & \text{when } i \neq j \end{cases} \tag{7}$$

i.e., c_1 is perpendicular to the plane formed by e_2°, e_3° and form an angle a with e_1°. e_1° is perpendicular to the plane formed by c_2° and c_3°. The other cases follow similarly. cos a_i is the direction cosine of the corresponding axis.

The gyro or acceleration meter is fixed on the vehicle along the six axes $e_1^\circ, e_2^\circ, e_3^\circ, c_1^\circ, c_2^\circ, c_3^\circ$. The data measured are $\Omega_i (i = e_1, e_2, e_3, c_1, c_2, c_3)$, respectively. Assume that there exists a space vector $\bar{\omega}$, then the projections of the vector $\bar{\omega}$ along the six axes are $\Omega_{e_1} = \bar{\omega} \cdot e_1^\circ$; $\Omega_{c_1} = \bar{\omega} \cdot c_1^\circ$ measured by the meters on them. $\bar{\omega}$ may be decomposed into three components along $e_1^\circ, e_2^\circ, e_3^\circ$ directions with size e_1, e_2, e_3 . Similarly, it may be decomposed along the $c_1^\circ, c_2^\circ, c_3^\circ$ directions with sizes c_1, c_2, c_3 . From equation (7), we know that c_2 and c_3 are normal to e_1. Hence, $\Omega_{e_1} = c_1 \cos a_1$. Similarly

$$\begin{bmatrix} \Omega_{e_1} \\ \Omega_{e_2} \\ \Omega_{e_3} \end{bmatrix} = \begin{bmatrix} \cos a_1 & 0 & 0 \\ 0 & \cos a_2 & 0 \\ 0 & 0 & \cos a_3 \end{bmatrix} \begin{bmatrix} c_1 \\ c_2 \\ c_3 \end{bmatrix} \tag{8}$$

Equation (8) may be written in matrix form $\Omega_e = DC$, 36

or
$$C = D^{-1}\Omega_e \tag{9}$$

Similarly $\Omega_e = DE$, or

$$E = D^{-1}\Omega_e \tag{10}$$

The angles a_{12}, a_{23}, a_{31} between the three axes $e_1^\circ, e_2^\circ, e_3^\circ$ of the non-orthogonal system are known and should be original parameters. The measured values $\Omega_{e_1}, \Omega_{e_2}, \Omega_{e_3}$ may also be expressed as the sum of the projections along this measurement axis of the three components e_1, e_2, e_3.

$$\begin{bmatrix} \Omega_{e_1} \\ \Omega_{e_2} \\ \Omega_{e_3} \end{bmatrix} = \begin{bmatrix} 1 & \cos a_{12} & \cos a_{31} \\ \cos a_{12} & 1 & \cos a_{23} \\ \cos a_{31} & \cos a_{23} & 1 \end{bmatrix} \begin{bmatrix} e_1 \\ e_2 \\ e_3 \end{bmatrix} = T \begin{bmatrix} e_1 \\ e_2 \\ e_3 \end{bmatrix} \tag{11}$$

Substituting equation (10) into equation (11), we get the value $\hat{\Omega}_e$ from which Ω_e is estimated with the measured value Ω_c.

$$\begin{bmatrix} \hat{\Omega}_{e1} \\ \hat{\Omega}_{e2} \\ \hat{\Omega}_{e3} \end{bmatrix} = TD^{-1} \begin{bmatrix} \Omega_{c1} \\ \Omega_{c2} \\ \Omega_{c3} \end{bmatrix} \tag{12}$$

$\because \Omega = DE$, according to equation (11), $E = T^{-1}\Omega_e$, hence

$$\begin{bmatrix} \hat{\Omega}_{e1} \\ \hat{\Omega}_{e2} \\ \hat{\Omega}_{e3} \end{bmatrix} = DT^{-1} \begin{bmatrix} \Omega_{e1} \\ \Omega_{e2} \\ \Omega_{e3} \end{bmatrix} \tag{13}$$

After the angles a_{ij} of the non-orthogonal system are determined, a_1, a_2, a_3 may be uniquely determined through solid geometrical relations. The difference ε_i between the estimated value $\hat{\Omega}_i$ and the measured value Ω_i may be formed from equations (12) and (13)

$$e_i = \Omega_i - \hat{\Omega}_i, \quad i = e_1, e_2, e_3, c_1, c_2, c_3, \tag{14}$$

A critical region W_a may be set up so that if $|e_i| \leqslant W_a$, it is normal and $e_i = 0$ but if $|e_i| > W_a$ then it is faulty and $e_i = 1$. If Ω_{c1} is faulty, then according to equations (12) and (13)

$$\begin{cases} e_1, e_4, e_5, e_6 = 1 \\ e_2, e_3 \qquad\quad = 0 \end{cases}$$

The other cases are similar. Based on the regularity of the appearance of 0-1, we can determine and isolate the fault of any gyro.

The common weakness of the dodecahedron method and the non-orthogonal method is:

(1) The principal environmental stresses have not been taken into consideration. For example, the visual acceleration W_{x1} along the longitudinal axis is more important for the vehicle, while the visual accerlations W_{y1}, W_{z1} along the transverse axes are very small.

Let the constant drift of a certain gyro with two degrees of freedom to be 1°/hr, and its overload drift to be 1°/hr g_o. When

applied to an ICBM, the spread caused is shown in Table 1.

TABLE 1

陀螺角动量$\bar{H}$的方向	x_1		y_1		z_1	
2 角漂移公式δ_o	$K_o+K_1\dot{W}_{y1}+K_2\dot{W}_{z1}$		$K_o+K_1\dot{W}_{z1}+K_2W_{x1}$		$K_o+K_1W_{x1}+K_2\dot{W}_{y1}$	
3 测量角速	ω_{y1}	ω_{z1}	ω_{z1}	ω_{x1}	ω_{x1}	ω_{y1}
4 引起漂移的主要项	K_o	K_o	$\dot{W}_{z1}$	$\dot{W}_{x1}$	$\dot{W}_{x1}$	$\dot{W}_{z1}$
5 引起散布（公里）	5.6	39.3	70.0	1.4	1.4	13.4

1--direction of the angular momentum H; 2--angular drift formula; 3--measured angular accelertion; 4--the principal term causing the drift; 5--induced spread

From the above table, it can be seen that the y_1 gyro measures w_{z1} and the z_1 gyro measures w_{y1}. Due to the effect of $\dot{W}_{x1}$, their errors are twice that of the x_1 gyro. If the direction of the angular moment $\bar{H}$ of the x_1 gyro deviates from the x_1 axis, then the component $\dot{W}_{x1}$ will be involved, causing a larger error, while the errors for the y_1 gyro and the z_1 gyro can only be minimized in measuring ω_{x1}. Similar situations hold true for the acceleration meter also. Accordingly, large errors will be introduced through the use of a non-orthogonal coordinate system or dodecahedron which should only be used when accuracy is not a concern. The key element affecting guidance accuracy (such as longitudinal acceleration meter) should have multiple installations along the optimal direction so that accuracy and reliability may be effectively enhanced. The transverse acceleration meter is not a key element and may be cut off when it becomes faulty without much effect. Hence, there is no need for duplication. 37

(2) Use of dodecahedron or non-orthogonal coordinate system methods may easily produce a wrong diagnosis. If two fault data are not very different among n pieces of data or one piece of data with large deviations is not much different from another piece of normal data but very different from other pieces of data, then

confusion will appear in the 0-1 combinations. In particular, when installation directions are not the same, some meters are more sensitive to environmental stresses, thus causing even more confusion.

(3) The computation is more complicated when one uses the dodecahedron or the non-orthogonal coordinate system method.

Due to the above mentioned causes, we propose in this paper that by installing multiple units of key elements along optimal directions, both accuracy and reliability will be enhanced. Attitude stabilizing systems may be duplicated orthogonally or non-orthogonally to enhance only reliability without duplicating the secondary parts. The method for fault-checking will be described below:

III. Fault-checking by polar difference

1. Principle of checking by polar difference

There are generally two forms of gyro error, one with no output (broken line, broken electric source) and the other the fast rotation phenomenon (damaged meter or appearance of extremely large positive or negative deviations). The first type of faults is easy to check. If there is no positive or negative pulse from a dynamic pressure gyro (no voltage after rectification), then it means a broken line or broken electric power source. To check for the fast rotation phenomenon, it is simpler to use the polar difference method.

Under the same conditions, because the data have random errors, the largest value x_{max} and the smallest value x_{min} of n measured values $x_1, x_2, \ldots, x_n$ are also random. The polar difference W for this set of measurements is

$$W = x_{max} - x_{min}$$

The sample polar difference is a random variable. Let it be after

$$W = (x_{max} - x_{min})/\sigma$$

after normalization.

Let the real values of a specific set of measurements be represented by

$$W_o=(x_{max}-x_{min})/\sigma \tag{15}$$

Now let a certain critical region W_a be defined. If $W_o \geq W_a$, then we consider the data to be faulty. If $W_o \leq W_a$, then we consider the n pieces of data are all normal.

Under the condition that the volume is n, the probability model that the random polar difference W_o is greater than some assumed value W may be derived with a multinomial distribution formula.

Let the probability density function of x be f(x). Let n data be measured, any one of which has the same probability of falling on the smallest value. Let this value be x. Its probability is nf(x). The other n-1 data will all fall in the range [x,x+W] with probability $\left[\int_x^{x+W} f(u)du\right]^{n-1}$. As x varies in the range $-\infty \sim +\infty$ then the probability that n data satisfy the polar difference is $n\int_{-\infty}^{\infty} f(x)\left[\int_x^{x+W} f(u)du\right]^{n-1}$. Its complementary event is that one or more of the n data will fall outside the polar difference W_a with probability $P(W>W_a|n)$. Let it be a, i.e.,

$$P(W>W_a|n)=1-n\int_{-\infty}^{\infty} f(x)\left[\int_x^{x+W_a} f(u)du\right]^{n-1}dx=a \tag{16}$$

In the above equation, if a is specified, then there is only one unknown Wa left. The result of solving the equation is shown in Table 2 [3]. That is to say that with normal data $W \leq W_a$. If $W>W_a$, then we have a small probability event (one possibility is sudden ineffectiveness, and the other is large deviation). We should then discard the pair of data x_{min}, x_{max}. One of the two pieces of data may be a normal one. Wouldn't it be a waste to discard it? It may be proved in sequential statistical theory that when the errors of the peripheral terms are large, there is no advantage in including them for accuracy calculations. On the other hand, by discarding them we may achieve two goals: (1) reliability will be improved by discarding ineffective data; (2) accuracy will be enhanced by discarding data with large errors. After the first round of

TABLE 2

W_a / a \ n	2	3	4	5	6	7	8	9
0.05	2.77	3 31	3 63	3.87	4.03	4.17	4.28	4.39
0.10	2.33	2 90	3.24	3 48	3.66	3.81	3 92	4 04
0.15	2.04	2.63	2.98	3.23	3.42	3.57	3.70	3.81

checking, the ineffectiveness will have been lowered by several orders of magnitude. For if to be further lowered, the remaining data may be checked for a second time with critical region determined by the method in [3].

For example, when sample volume n = 4 (with four acceleration meters), take a = 0.1 to get W_a = 3.24 from the table. Thus, the probability that the polar difference is greater than 3.24 σ should be less than 10%. Hence, we discard this pair of data. If the sensors possess a regular error $\gamma\sigma$ with half installed normally and the other half reversed and backward, then the critical region may be taken as $W_a = (3.24 + 2\gamma)\sigma$.

a is to be determined according to the actual situation. If a is too large, then type 1 error will be made (treating normal data as abnormal) with a high probability, while if a is too small, then it is easy to introduce data with large deviations, therefore, committing a type 2 error.

After polar difference checking with faulty data or data with large deviation discarded, the unreliability defect of the arithmetic averaging method will be solved.

2. Ineffectiveness checking using polar difference

In n pieces of data measured by n instruments, at least (n+1)/2 (take integer value) will be ineffective and at least (n+1)/2 ineffective data will all be either greater or smaller than the real values, i.e., the system will fail when all the errors are one-sided. (Note: this situation is hard to check even with 0-1 checking since

the data with a large deviation may be close to one another). The probability that each data is larger or smaller is respectively 1/2. For (n+1)/2 or at least (n+1)/2 ineffective data to be one-sided, the formula for the total probability that the system be ineffectiveness is

$$Q_p = C^n_{\left[\frac{n+1}{2}\right]} q^{\left[\frac{n+1}{2}\right]} (1-q)^{n-\left[\frac{n+1}{2}\right]} \left(\frac{1}{2}\right)^{\left[\frac{n+1}{2}\right]-1}$$

$$+ C^n_{\left[\frac{n+1}{2}\right]+1} q^{\left[\frac{n+1}{2}\right]+1} (1-q)^{n-\left[\frac{n+1}{2}\right]-1} \left(\frac{1}{2}\right)^{\left[\frac{n+1}{2}\right]}$$

39

$$\cdot\left(1 + C_1^{\left[\frac{n+1}{2}\right]+1}\right) + C^n_{\left[\frac{n+1}{2}\right]+2} q^{\left[\frac{n+1}{2}\right]+2} (1-q)^{n-\left[\frac{n+1}{2}\right]-2} \tag{17}$$

$$\cdot\left(\frac{1}{2}\right)^{\left[\frac{n+1}{2}\right]+1}\left(1 + C_1^{\left[\frac{n+1}{2}\right]+2} + C_2^{\left[\frac{n+1}{2}\right]+2}\right) + \cdots\cdots + q^n$$

Ordinarily n is not too large. When the ineffectiveness of an individual instrument to be less than a few percent, equation (17) may be simplified as

$$Q_p = 2^{1-\left[\frac{n+1}{2}\right]} C^n_{\left[\frac{n+1}{2}\right]} q^{\left[\frac{n+1}{2}\right]} \tag{18}$$

It should be explained that when the polar difference is outside the critical region for n = 2, if data closer to the theoretical standard is selected, then the system will fail only when both data are ineffective. This is an exception to equation (18).

TABLE 3

n	1	2	3	4	5	6	7	8	9	10
Q_p	q	q^2	$1.5q^2$	$3q^2$	$2.5q^3$	$5q^3$	$\frac{35}{8}q^4$	$\frac{35}{4}q^4$	$\frac{63}{8}q^5$	$\frac{63}{4}q^5$

If the rate of failure of a single instrument is 1%, then with n instruments, the rate of failure will be lowered by $2^{\left[\frac{n+1}{2}\right]-1}$ order of magnitude.

3. The accuracy in averaging the normal data after polar difference checking.

Element failure may be divided into two types. One is sudden failure, meaning that a fast rotation is caused by the failure of one part. The other is property failure, meaning that error may become larger than the critical range W due to the accumulation of random interference with the same sign. The former is discussed under reliability in equation (17), while the latter is discussed under accuracy analysis, derived as follows.

Let n numbers be measured. Two cases will be differentiated. One case is that polar difference checking is normal. The probability of occurrence of this case is 1-σ. After arithmetic averaging, the mean square deviation is σ_{1-a}; the other case is that polar difference checking has not passed. The probability of occurrence for this case is a. If the disqualified data are not discarded, the mean square deviation after averaging is σ_a.

The above two cases combine to be ordinary arithmetic averaging, namely,

$$\frac{\sigma}{\sqrt{n}} = \sqrt{\sigma_{1-a}^2(1-a)+\sigma_a^2 a} \tag{19}$$

Apparently

$$\sigma_a > \frac{\sigma}{\sqrt{n}} > \sigma_{1-a} \tag{20}$$

If polar difference checking has failed, after discarding the disqualified data, the mean square deviation after averaging is σ_α^1 Let us discuss the worst condition for σ_α. The worst situation is to select the median of the sequential data (i.e., arranging the data sequentially from small to large, take the middle value for odd number of values, and the average of the middle two values for even

number of data). In reference [4], it is proved that n < 10 the worst situation $\sigma_e = 1.2\frac{\sigma}{\sqrt{n}}$. From [6] page 421 example 6-2, it is also proved that the mathematical expectation and square deviation of a simple median approach is respectively m and $\frac{\pi}{2n}\sigma^2$. From this one obtains 40

$$\sigma_e \leq \sqrt{\frac{\pi}{2}}\ \frac{\sigma}{\sqrt{n}} = 1.25\frac{\sigma}{\sqrt{n}} \tag{21}$$

Hence, the worst combined mean square deviation σ_1 is

$$\sigma_p = \sqrt{\sigma^2_{1-\alpha}(1-\alpha) + 1.25^2\frac{\sigma^2}{n}\alpha} < \sqrt{\frac{\sigma^2}{n}[1-\alpha+1.25^2\alpha]}$$

If we let a = 0.1, then

$$\sigma_p < 1.025\frac{\sigma}{\sqrt{n}} \tag{22}$$

From this it may be concluded that polar difference checking has greatly enhanced reliability, with accuracy approaching that of arithmetic averaging, i.e., by $\frac{1}{\sqrt{n}}$ times with the worst case not to exceed $\frac{1.025}{\sqrt{n}}$

IV. Examples

Example 1. Method with three sets of duplications

Method 1. The middle value is selected directly without polar difference checking. For instance, integrate the vehicle acceleration with three acceleration integrators. When the present velocity is reached, an engine shut-off command is issued. As there exist random errors in all three integrators, the issuing of the engine shut-off commands will not be at the same time. Only when the second command has been received will the engine be actually shut down. Here the computational setup may be saved, since polar difference checking is not necessary.

Method 2. Arrange the data measured in real time from small to large as x_1, x_2, x_3.

and when $\begin{cases} x_3 - x_1 \geq \Delta'_e & \text{take } x_2; \\ x_3 - x_1 \leq \Delta'_e & \text{take } x = \frac{1}{3}(x_1 + x_2 + x_3) \end{cases}$

Method 3. Select $x=\frac{1}{3}(x_1+x_2+x_3)$ without checking. The three methods are compared as follows:

	1 单 台	2 普通算术平均	3 取 中 值	4 极差检验
5 均方差 σ_p	σ	0.577σ	0.6698σ	0.577σ
6 失效率 Q_p	q	$3q$	$1.5q^2$	$1.5q^2$

1--single meter; 2--ordinary arithmetic averaging; 3--median value; 4--polar difference checking; 5--mean square difference σ_p; 6--failure rate Q_p

Example 2. With four duplication sets, the accuracy with averaging after polar difference checking is enhanced one fold comparing to that of a single meter. The failure rate is $3q^2$. It should be pointed out that when there exist unknown regular errors for the single meter, there are two factors m and σ in measuring the accuracy of the single meter. Now the probability for satisfying the condition that the maximum error is to be within the range Z_{max} is 99.3%. If the regular error $m = 0$, then the single meter accuracy is required to be $\sigma=Z_{max}/2.7$. When $m \neq 0$, what should be the single meter accuracy σ_2 so that the requirement that the probability range be within the allowed limits may be satisfied? Let $m = r\sigma_x$, $\sigma_x = \beta\sigma$, the following equation should be satisfied

41

$$\int_{-2.7\sigma}^{2.7\sigma} \frac{1}{\sqrt{2\pi}\,\beta\sigma} e^{-(x-\gamma\beta\sigma)^2/2(\beta\sigma)^2}\, dx = 99.3\%$$

which may be solved to get

γ	0	0.5	0.8
β	1	0.911	0.824

With four identical elements, half of it installed normally and the other half reversed and backward, the regular error is basically eliminated. With polar difference checking average, the random error is halved, so that the accuracy is enhanced to

γ	0	0.5	0.8
accuracy enhancement	0.5	0.456	0.412

In space vehicle design, the guidance error caused by the error in the longitudinal axis acceleration meter is one order of magnitude larger than in other directions. If we install four duplicate meters in this direction, the accuracy of the whole system will be equivalently enhanced one fold, and the accuracy is also greatly enhanced.

Example 3. Realistic duplication method of strap-down guidance system. Duplicate signals for pitch, yaw and roll angles may be measured with three gyros with two degrees of freedom. Duplicate signals for longitudinal acceleration may be measured with two longitudinal acceleration meters. A transverse acceleration meter is secondarily important and will not be duplicated. When the duplicate signal polar difference exceeds the critical value, the data closer to the theoretical standard will be selected. When the polar difference is less than or equal to the critical value, the average of the two values is selected. In this way, although one acceleration meter and one gyro with two degrees of freedom are added, the guidance error is reduced by $\frac{1}{\sqrt{n}}$ times, and the failure rate by two orders of magnitude. When this kind of setup is installed in vehicles with a fast engine propeller, there will be no need to change elements if it should be discovered before launching that some inertial element may be faulty so that time will not be lost.

REFERENCES

[1] Hung, I.C., *Progress in Strapdown Technology*, Tennesee 37916 U S.A..

[2] Robert, C.K. Lee, "The Application of Nonorthogonal Coordinates to Improve the Reliability and Performance of a Spacecraft Attitude," AIAA Journal.

[3] E.S. Peason and H.O. Hartley, "Biometric for Statisticians," Vol. 1, p. 43, p. 178, 1966.

[4] He Lucheng. Application of Statistical Experimental Method in Accuracy Analysis. Journal of the Study and Implementation of Mathematics, 1, 1975.

[5] Yamaguchi Jiro. Statistical Table and Formuluae with Computer Applications, JSA, 1972.

[6] M. Fisher. Probability Theory and Mathematical Statistics. Translated by Wang Fubao, Science and Technology Publisher, Shanghai 1962.

THE RESEARCH OF THE PROJECT FOR ADJUSTING THE THRUST OF SOLID ROCKET PROPULSOR

Xu Wengan

Abstract

A conception of adjustable solid propellant rocket motor was proposed. It is going to be achieved through the use of propellants having negative pressure exponent n. In this paper, the feasibility of the technique and characters of adjustment were discussed. Other advantages of the propellent with a negative pressure exponent were also presented.

SYMBOL TABLE 43

A_b	combustion surface area
A_t	jet throat area
a	combustion rate coefficient
C^*	characteristic speed
C_F	thrust coefficient
C_i (i=1,2)	constants
F	thrust
F_{max}	maximum thrust
F_g	given thrust
k	specific heat ratio of fuel vapor
K_i (i=1,2)	constant coefficients (including those with superscript ",","","",)
n	combustion pressure index
P_c	combustion chamber pressure
r	combustion rate
t	time
u(t)	unit step function
V_c	combustion chamber volume
a	$(=\lambda/\rho c)$ propellant thermal diffusion rate
Γ	function of k
$\bar{\varepsilon}(\infty)$	static difference
λ_i (i=1,2)	constant coefficients
ρ_c	fuel vapor density
ρ_p	propellant density
σ	superharmonics
$\tau_{0.05}$	transition time

I. Introduction

Much work has been done both internationally and domestically on the thrust control of solid propellant rocket engines, resulting in the development of such direction control systems and thrust termination mechanisms based on various action principles as "inclined flow ring", "rotating jet", "vibrating jet", "soft jet", "liquid float jet" and "secondary injection" of liquid of fuel vapor, etc.

*Received 2 September 1980

However, there is as yet no good and practical method for regulating the strength of thrust. Although there have been some proposals such as "layered engine" to inject certain liquids into the combustion chamber and some preliminary attempts in applying methods of installing a regulating cone in the jet or making use of propellant with n greater than 0 and close to 1 with a mechanical rotating valve based on propellants with positive pressure coefficients [1] [2], yet little prospect can be seen due to the complexity in the structure and the bad weight and service properties. 44

In this paper, we shall attempt to investigate the possibility of solving this problem by using new propellants with pressure coefficient less than 0, but absolute value greater than 1 (for convenience of discussion, we shall call them by the name "high negative pressure" propellant).

II. The feasibility and advantage of implementing thrust control by "high negative pressure propellant"

Why do we want to study this kind of propellant? Will this kind of propellant provide the feasibility of implementing thrust regulation? What are the advantages? Apparently, these questions should be answered first. As is well known, when the combustion rate obeys the equation $r = ap_c^n$, and the sound speed flow exists in the jet throat, the balanced pressure and the corresponding thrust of the solid fuel rocket engine combustion chamber may be expressed with the two equations below:

$$P_c = \left(\rho_p \cdot C^* \frac{A_b}{A_t} \cdot a \right)^{\frac{1}{1-n}} \qquad (1)$$

$$F = C_f P_c A_t \qquad (2)$$

From the equations above, it can be seen that once the propellant has been selected, the only effective way to regulate the thrust is to vary the parameters A_b and A_t. Of the two, the parameter that allows one to randomly vary it by simple means (i.e., the kind of

parameter that is varied not according to a preset program, but according to current need) is basically the jet nozzle throat area A_t. Hence, we shall vary equations (1) and (2) simultaneously to obtain the equations below as the basic equations in this paper:

$$P_c = K_1 A_t^{\frac{1}{n-1}} \qquad (3)$$

$$A_t = \left(\frac{F}{K_2}\right)^{1-\frac{1}{n}} \qquad (4)$$

$$P_c = K_3 F^{1/n} \qquad (5)$$

where

$$K_1 = (\rho_p \cdot C^* \cdot A_b \cdot a)^{\frac{1}{1-n}}$$

$$K_2 = C_F \cdot K_1$$

$$K_3 = K_1 \cdot K_2^{-\frac{1}{n}}$$

When the propellant is already determined and the combustion area A_b is a constant, it is apparently permissible to use K_1 as a constant in the analysis. C_F is also obviously a function of A_b/A_t and P_c, but in the confines of our discussion here, it may be taken approximately as a constant. Thus, we shall treat K_2, K_3 approximately as constants below. In this way, by differentiating logarithmically both sides of the equations above, we obtain

$$\frac{dp_c}{p_c} = \frac{1}{n-1}\frac{dA_t}{A_t} \qquad (6)$$

$$\frac{dA_t}{A_t} = \left(1-\frac{1}{n}\right)\frac{dF}{F} \qquad (7)$$

$$\frac{dp_c}{p_c} = \frac{1}{n}\frac{dF}{F} \qquad (8)$$

45

From equations (5) or (8), we know that in order to regulate the thrust, it will be necessary to alter the pressure in the combustion chamber. But when the variation in pressure becomes unacceptable in practice, the regulation of the thrust will also become an empty dream. Hence, we must try to minimize the pressure variation of the combustion chamber during thrust regulation (thus taking full advantage of the structural strength of the engine), and maximize the absolute value of n. For example, when the pressure index n = 0.75, the pressure must be increased 16 times or 6.34 times,

respectively, in order to increase the thrust by 8 or 4 times. Changes of this magnitude will naturally lower the weight property of the engine when we want to make sure that it will operate under the highest pressure. This is also the point of vulnerability in some of the experiments and design reported in some countries. But when n = -2, to increase the thrust by the same factor, the pressure needs to be reduced only to 1/3.83 or 1/2 of the original pressure. Obviously, the situation is greatly improved and the combustion chamber pressure variation significantly reduced.

From the above consideration, it is apparent that the larger |n| is, the better. However, in order to keep the engine operating stably, a n value with absolute value greater than 1 cannot be positive because when the flow rate of the engine is equal to the rate of generation of the fuel vapor, it operates under equilibrium pressure (p_{cb}) and for this equilibrium, like all other equilibrium problems, there exist stable, unstable and neutral states. If due to the effect of some random factor the combustion chamber pressure deviates from the equilibrium pressure P_{cb}, then will there be a tendency to diminish this deviation, or a tendency to increase this deviation? Or will equilibrium be established under the new conditions? These are then the difference between the three types of equilibria. For the engine to operate stably, we must have stable equilibrium. The mathematical expression for this analysis may be:

$$\frac{d}{dp_c}\left(\frac{dp_c}{dt}\right)<0 \quad (1)$$

where

$$\frac{dp_c}{dt}=\frac{\Gamma^2 C^{*2}}{V_c}\left[(\rho_p-\rho_c)A_b a p_c^{n}-\frac{A_t \rho_c}{C^*}\right]$$

$$\frac{d}{dp_c}\left(\frac{dp_c}{dt}\right)=\frac{\Gamma^2 C^{*2}}{V_c}\left[(\rho_p-\rho_c)A_b a n p_c^{n-1}-\frac{A_t}{C^*}\right]$$

At the equilibrium point, we have

$$(\rho_p-\rho_c)A_b a p^{n}=\frac{A_t p_c}{C^*}$$

Substituting into the above equation, we obtain

$$\frac{d}{dp_c}\left(\frac{dp_c}{dt}\right)=\frac{\Gamma^2 C^{*2}}{V_c}\cdot\frac{A_t}{C^*}[n-1]$$

Also because

$$\frac{\Gamma^2 C^{*2}}{V_c}\cdot\frac{A_t}{C^*}>0$$

Hence in order that

$$\frac{d}{dp_c}\left(\frac{dp_c}{dt}\right)<0$$

We must let $n - 1 < 0$ 46

i.e., $n < 1$

This may be seen intuitively from Figure 1.

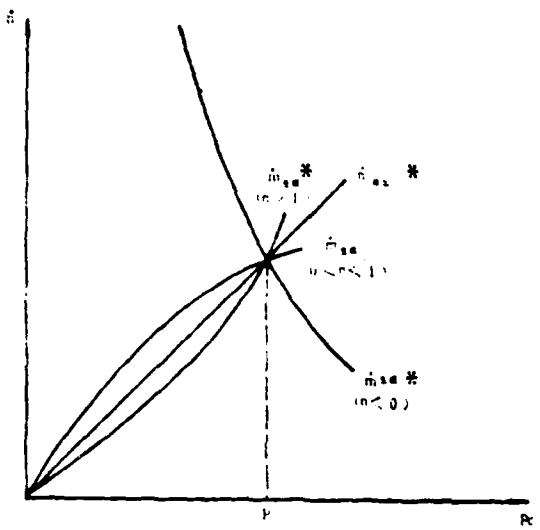

Figure 1

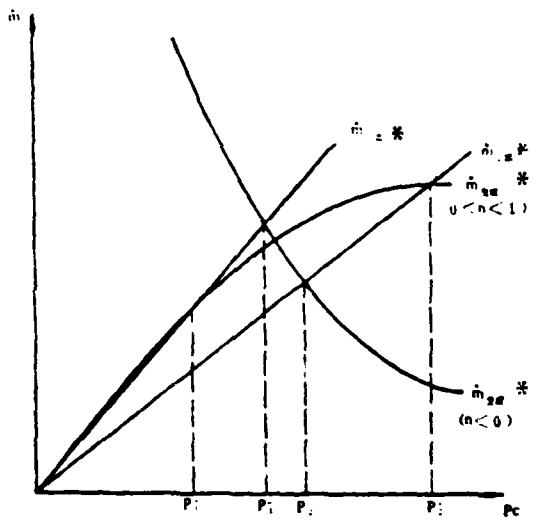

Figure 2

*Translator's note: illegible in foreign text.

Hence, we should use "high negative pressure index" propellant so as to minimize the variation of the combustion chamber pressure during thrust regulation.

---

(1) (for pg. 73) $\frac{d}{dp_c}\left(\frac{dp_c}{dt}\right)$ is just the common mathematical expression $\frac{d^2t}{dp_c^2}>0$. since the former may become

$$\frac{d}{dp_c}\left(\frac{1}{\frac{dt}{dp_c}}\right)<0 \qquad \text{i.e.} \qquad \frac{-\frac{d^2t}{dp_c^2}}{\left(\frac{dt}{dp_c}\right)^2}<0$$

or $\frac{d^2t}{dp_c^2}>0$

At the same time, differentiating both sides of equation (1) logarithmically, we find from equations (1), (2) that

$$\frac{dp_c}{p_c} = \frac{1}{1-n}\left[\frac{d\rho_p}{\rho_p} + \frac{dC^*}{C^*} + \frac{dA_b}{A_b} - \frac{dA_t}{A_t} + \frac{d_a}{a}\right] \qquad (9)$$

It can be seen that fluctuations in the parameters ρ_p, C^*, A_b, A_t, a induced by some factor will also cause the combustion chamber pressure p_c and the thrust F to fluctuate and when the relative fluctuation of the former is fixed, that of the latter will decrease with decreasing n value. In practice, among the above parameters (i.e., ρ_p, C^*, A_b, A_t, a the combustion rate coefficient a fluctuates the most. Based on the demand of practical fuel rod production, it is often permitted to vary over a wide range. For example, in the two typical ways of preparing mixture propellant, the values of $\Delta a/a$ are specified respectively to be about 0.07 and 0.02 which is already fairly difficult in the industry. But if n = 0.75, then together with the fluctuations of other parameters, $\Delta p_c/p_c$ may reach as high as 0.28 and over 0.08, respectively. However, if n = -2, then $\Delta p_c/p_c$ will be respectively reduced to 0.023 and 0.007. The advantage is obvious. It can significantly decrease the fluctuation in the combustion chamber pressure and the spread of engine thrust.

Besides the effect of $\Delta A_b/A_b$ on $\Delta p_c/p_c$ can also be reduced significantly, thus permitting the design of fuel rods with large area ratio to increase the fuel insertion density of the engine.

Summarizing the above discussions, as shown in Figure 2, by using a new "high negative pressure index" propellant, it is possible to regulate thrust within a wide range without altering the current basic structure of the solid propellant rocket engine. It also possesses the advantage of reducing the fluctuation in combustion chamber pressure and the spread in engine thrust and increasing the density of fuel rod insertion. 47

Of course, in order to implement the regulation of thrust, it is also necessary to be able to regulate over a wide range the area

of the nozzle throat. It can be observed from equations (4) and (7) that when $n < 0$ and $|n| > 1$, one needs to vary the nozzle throat area A over a large range to obtain the required thrust regulation range. In the two examples cited, the thrust is increased eight-fold in both cases. For $n = 0.75$, A needs only be reduced by one-half, while for $n = -2$, A needs to be increased by more than 22.6 times its original value. This is inconceivable in the ordinary design of the mechanical regulation of nozzle throat area. But this is not a problem when "vortex flow valve" of the flow control type is used. As the energy of the propellant is improved constantly, it is only through the flow control technology that the nozzle throat area (hence the flow volume) may be regulated under the bad working condition of the nozzle throat. Hence, theoretically this need is not an impediment to the implenetation of thrust regulation in our design. On the contrary, it actually provides the feasibility that, as one part of the automatic regulation system, it will achieve the accuracy and static characteristics desired.

III. Can "high negative pressure index" propellant be obtained?

Limited by the study, we are not yet able to give a quantitative analysis based on combustion mechanism. We shall only mention the following points as a basis in our discussion:

1. Propellants with $n < 0$ already exist not only theoretically, but also in practice. In one preparation, a pressure range of 50-70 kg/cm and pressure index $n = -0.825$ has been achieved.

In the reports on double-base platform propellant and mixed material propellant overseas, the so-called "mesa effect [3,5] with $n < 0$ has appeared. Recently, there have been reports on mixed material propellant with $n < 0$ and even $n = -4.0$ [4]. This demonstrates that it is feasible and practical to obtain "high negative pressure index" propellants.

2. In many foreign references, [1,4,5,6], the mechanism of the "mesa effect" in the combustion of mixed material solid propellant has been discussed.

(1) From the microfilm of the combustion surface after experimental ignition shut-off, it can be observed that at low pressure (less than 30 kg/cm), the surface of ammonium chlorate (Ap) crystals is convex, since the thermal dissociation of the adhesive under this condition is faster than that of Ap, while at high pressures (greater than 30 kg/cm), the surface has concave pits, indicating that the Ap crystals are consumed faster [1].

(2) p-amino ester (pU) is different from the adhesive carboxyl p-butadiene (CTPB) in that it already becomes very fluidized before the temperature for its rapid dissociation is reached, while the latter is a highly adhesive foamy fluid. Under high pressure, local quenching [1,4,5,6] will occur when an easily fluidized adhesive flows over and covers the surface of Ap crystals that dips below the combustion surface.

(3) It has been observed with the movie camera method that irregular pulsed combustion with partial quenching has appeared in platform propellants. The area of this local quenching as a fraction of the total area determines the degree of decrease of the combustion rate averaged over the whole combustion surface. The dependence of this fraction on the pressure is what causes the decrease of the pressure index n until the appearance of the "mesa" effect with $n < 0$ [1,4,5].

(4) When salt that melts easily such as $(NH_4)_2SO_4$ is added to the propellant as combustion speed regulator, the local quenching phenomenon can also be induced. Or the dissociation of NH_4ClO_4 may be suppressed [4] due to the NH_4^+ ions and a deep thermal potential hill.

3. In [4], a physical picture verified by some expeirmental observations is proposed for the combustion process of this kind of propellant.

An engine experiment using 80 lb. of propellant with n = -2.5 is also reported.

IV. Preliminary analysis of some regulatory properties

48

For the overall cycle of thrust auto-regulating systems, the regulation of the engine is only one link. However, its regulatory properties obviously should be analyzed.

For convenience, let us assume that the combustion rate still obeys the law $r = ap_c^n$ during the regulatory process, that at all times sound velocity flow exists at the nozzle throat, and that the pressure in the combustion chamber is the same everywhere and is also equal to the pressure at the nozzle inlet. Thus, we get from the continuity equation of the fuel vapor:

$$\frac{d\rho_c}{dt} = \frac{\Gamma^2 C^*}{V_c}\left[(\rho_p - \rho_c)A_b a p_c^n - \frac{A_t \rho_c}{C^*}\right] \tag{10}$$

Again by differentiating equation (2) logarithmically with C_F a constant, we get

$$\frac{dF}{F} = \frac{d\rho_c}{\rho_c} - \frac{dA_t}{A_t}$$

and

$$\frac{1}{F}\frac{dF}{dt} = \frac{1}{\rho_c}\frac{d\rho}{dt} - \frac{1}{A_t}\frac{dA_t}{dt} \tag{11}$$

By solving simultaneously equations (2), (10) and (11), we can obtain the dynamic equation for this part as

$$\frac{1}{F}\frac{dF}{dt} = K_1\left(\frac{F}{A_t}\right)^{n-1} - K_2 A_t + \frac{1}{A_t}\frac{dA_t}{dt} \tag{12}$$

where

$$K_1 = \frac{\Gamma^2 C^{*2}}{V_c} - (P_b - P_c) A_t a C_F^{-n}$$

$$K_2 = \frac{\Gamma^2 C^*}{V_c}$$

When the input is a unit step function, i.e., $A_t = A_{t_0} + u(t)$ (A_{t_0} is the nozzle throat area before the unit step function action) apparently $dA_t/dt = 0$ and $u(t) = 1$ for $t > 0$. By differentiating equation (12), we get

$$\frac{dF}{dt} + K_2' F = K_1' F^n$$

where

$$K_1' = \frac{K_1}{[A_{t_0} + 1]^{n-1}}$$

$$K_2' = K_2 [A_{t_0} + 1]$$

The differential equation obtained for this unit transition process, equation (13), is a typical Bernoulli equation. Hence, its solution may be obtained through the method of separation of variables. When $n \neq 1.0$,

$$t = \frac{-1}{(1-n)K_2'} \ln(K_1' - K_2' F^{1-n}) + C_1$$

From the initial conditions: $t = 0^+$, $F = F(0)$, we get

$$C_1 = \frac{1}{(1-n)K_2'} \ln\{K_1' - K_2' [F(0)]^{1-n}\}$$

Therefore,

$$t = \frac{1}{(1-n)K_2'} \ln \frac{K_1' - K_2' [F(0)]^{1-n}}{K_1' - K_2' F^{1-n}}$$

$$F(t) = \lambda_1 \{1 - \lambda_2 \exp[(n-1)K_2' t]\}^{\frac{1}{1-n}} \qquad (14)$$

where

$$\lambda_1 = \left(\frac{K_1'}{K_2'}\right)^{\frac{1}{1-n}}$$

$$\lambda_2 = 1 - (K_2'/K_1')[F(0)]^{1-n}$$

Also since $(n-1) < 0$, then from (14) we get, when $t \longrightarrow \infty$, $F(\infty) = \lambda_1$, and $\lambda_2 = 1 - \left[\frac{F(\infty)}{F(0)}\right]^{n-1}$. Hence equation (14) may also be written as

$$F(t) = F(0)\left\{1 - \left[1 - \left(\frac{F(0)}{F(\infty)}\right)^{1-n}\right] \exp[(n-1)K_2' t]\right\}^{\frac{1}{1-n}} \qquad (15)$$

1. Transition period: by definition $\frac{|F(\tau_{0.05})-F(\infty)|}{F(\infty)}=0.05$ we get

$$\tau_{0.05}=\frac{1}{(n-1)K_2'}\ln\frac{1-(1\pm0.05)^{1-n}}{1-\frac{F(0)}{F(\infty)}^{1-n}} \qquad (16)$$

where the + and - signs correspond respectively to the situations of $0 < n < 1$ and $n < 0$.

When the relative regulation is assumed to be

$$\Lambda=\frac{|F(\infty)-F(0)|}{F(\infty)}\cdot100\%=10\%$$

for the cases $n = 0.75$ and $n = -2$, $\tau_{0.05}$ is respectively about $1.43/K_2'$ and $0.213/K_2'$ which means that the transition period of the latter is only 1/7 of that of the former.

2. Super-regulation: From equation (14), we get $F_{max} = \lambda_1$. Therefore, by definition the super-regulation is

$$\sigma=\frac{F_{max}-F(\infty)}{F(\infty)}\cdot100\%=0.$$

3. Static difference: From the given value $F_g=P_{c_g}\cdot C_F\cdot[A_{t_0}+u(t)]$ and $P_{c_g}=\left[(\rho_g-\rho_c)\cdot C^*\frac{A_b}{A_{t_0}+u(t)}\cdot a\right]^{\frac{1}{1-n}}$, we can obtain $F_g=\left\{\frac{K_1'}{K_2'}\right\}^{\frac{1}{1-n}}=F(\infty)$. Therefore, by definition, the static difference $\varepsilon(\infty)=\frac{|F_g-F(\infty)|}{F_g}\cdot100\%=0$. (In the above P_{cg} is the static equilibrium pressure corresponding to a given thrust).

When the pressure changes rapidly, the combustion rate is no longer only a function of the pressure, but is also a function of the rate of change of the pressure, e.g., $r=ap_c^n\left(1+\frac{an}{a^2p_c^{2n-1}}\frac{dp_c}{dt}\right)$. (If we assume that the empirical equation can still be used for $n < 0$, we can obtain by the same token the corresponding dynamic equation for unit step process:

$$\frac{dF}{dt}=\frac{K''F^{n-1}-K'F^{n-2}}{K''F^{n-1}-K'^{n}}$$

When $n \neq 1.0$, its solution is

$$t = \frac{-1}{(1-n)K_2'} \ln(K_1' - K_2' F^{1-n}) - \lambda_1 n \left(\frac{dF}{F^{n+1} - \lambda_1 F^{n+2}} \right)$$

Experiments indicate [7] that the combustion rate pressure index n_a for instantaneous pressure change will still be greater than the pressure index n during slow change. Hence, the assumption above that the combustion rate during the regulatory process agress with $t = ap_c^n$ is obviously going to be quite different from reality. This difference may be seen from the empirical law shown in Figure 2 of reference [4]. Therefore, the above analysis is only preliminary.

REFERENCES

[1] "Fundamental Problems of Solid Propellant Rocket Engine" translated by Jing Guqun, vol. 1, p 361-362,352. Vol. 2, p. 412-414.

[2] M. N. Director and R. Polzien. "Development of a Thrust Modulated Solid Propellant Motor" AIAA 80-1221.

[3] "Collection of translated papers on platform propellant" edited and translated by the Hou 414 Battalion.

[4] J. Cohen, L. C. Landers and R. L. Lou. "Zero Time Delay Controllable Solid Propellant Gas Generators" Journal of Spacecraft and Rockets, May 1977 p. 310-314 or AIAA 76-691.

[5] J. A. Steinz, P. L. STand and M. Summerfield. "The Burning Mechanism of Ammonium Perchlorate-based Composite Solid Propellants" AD 688944 Feb. 1969.

[6] T. Godai, etc. "Pressure Exponent of Controllable Solid Rocket Propellants" AIAA 72-1135.

[7] B. Dubrow, E. D. Guth. "Ballistics of Solid Propellants during Thrust Modulation" AIAA 64-130.